

HMGA1 induces FGF19 to drive pancreatic carcinogenesis and stroma formation

Lionel Chia,^{1,2} Bowen Wang,^{2,3} Jung-Hyun Kim,² Li Z. Luo,² Shuai Shuai,² Iliana Herrera,² Sophia Y. Chen,⁴ Liping Li,² Lingling Xian,² Tait Huso,² Mohammad Heydarian,⁵ Karen Reddy,⁵ Woo Jung Sung,² Shun Ishiyama,^{6,7} Gongbo Guo,² Elizabeth Jaffee,⁸ Lei Zheng,⁸ Leslie M. Cope,^{8,9} Kathy Gabrielson,⁷ Laura Wood,^{1,6,8} and Linda Resar^{1,2,3,6,8}

¹Pathobiology Graduate Program, Department of Pathology and ²Division of Hematology, Department of Medicine, Johns Hopkins University School of Medicine, Baltimore, Maryland, USA. ³Biochemistry and Molecular Biology Program, Johns Hopkins Bloomberg School of Public Health, Baltimore, Maryland, USA. ⁴Department of Surgery, ⁵Department of Biological Chemistry, ⁶Department of Pathology, ⁷Department of Molecular and Comparative Pathobiology, ⁸Department of Oncology, and ⁹Division of Biostatistics, Sidney Kimmel Comprehensive Cancer Center, Johns Hopkins University School of Medicine, Baltimore, Maryland, USA.

High mobility group A1 (HMGA1) chromatin regulators are upregulated in diverse tumors where they portend adverse outcomes, although how they function in cancer remains unclear. Pancreatic ductal adenocarcinomas (PDACs) are highly lethal tumors characterized by dense desmoplastic stroma composed predominantly of cancer-associated fibroblasts and fibrotic tissue. Here, we uncover an epigenetic program whereby HMGA1 upregulates FGF19 during tumor progression and stroma formation. HMGA1 deficiency disrupts oncogenic properties in vitro while impairing tumor inception and progression in KPC mice and subcutaneous or orthotopic models of PDAC. RNA sequencing revealed HMGA1 transcriptional networks governing proliferation and tumor-stroma interactions, including the *FGF19* gene. HMGA1 directly induces *FGF19* expression and increases its protein secretion by recruiting active histone marks (H3K4me3, H3K27Ac). Surprisingly, disrupting *FGF19* via gene silencing or the *FGFR4* inhibitor BLU9931 recapitulates most phenotypes observed with HMGA1 deficiency, decreasing tumor growth and formation of a desmoplastic stroma in mouse models of PDAC. In human PDAC, overexpression of *HMGA1* and *FGF19* defines a subset of tumors with extremely poor outcomes. Our results reveal what we believe is a new paradigm whereby HMGA1 and FGF19 drive tumor progression and stroma formation, thus illuminating FGF19 as a rational therapeutic target for a molecularly defined PDAC subtype.

Introduction

Pancreatic ductal adenocarcinoma (PDAC) has emerged as a major public health problem in industrialized countries, and its incidence is rising (1–3). PDAC is predicted to become the second leading cause of cancer death in the United States by 2030, overtaking breast, prostate, and colorectal cancer (3). Most patients present with locally advanced or widely metastatic disease, rendering these tumors surgically unresectable (1–3). Even patients with localized tumors amenable to surgical resection will succumb to metastatic disease in almost all cases, suggesting that metastases occur prior to clinical presentation (1). Although previous studies identified mutant *KRAS* and molecular alterations inactivating *CDKN2A*, *TP53*, and TGF- β pathway components, these findings have not translated into improved therapies, nor have they led to effective screening strategies (3, 4, 5). Thus, there is a dire need to discover actionable mechanisms and new therapeutic targets for this exceptionally refractory tumor.

In contrast to many solid tumors, PDACs are characterized by a dense desmoplastic stroma composed of cancer-associated fibroblasts (CAFs) and fibrous scar tissue, although the role of the stroma in tumor progression remains controversial (6–11). While immune cells are found within the stroma, PDACs tend to be “cold” tumors, lacking an antitumor immune response (12). In vitro studies show that CAFs secrete factors that provide inflammatory signals and stimulate tumor growth and progression (9–11). Similarly, biomechanical analyses suggest that a “stiff” tumor microenvironment alters tumor cells to enhance motility and facilitate metastases (13–15). Further, PDAC cells grow faster when implanted with CAFs in mouse xenografts (16). The dense fibroblastic stroma also provides a barrier that prevents cytotoxic therapy from reaching tumor cells (9). Conversely, studies in transgenic mouse models of PDAC found that the stroma restrains tumor growth and progression (7, 8). More recent studies employing single-cell sequencing revealed that stromal cells, like cancer cells, are heterogeneous and impart tumor heterogeneity by creating various interfaces for tumor cells within their microenvironment (9, 17–23). These studies reveal a complex and nuanced role for the PDAC stroma, underscoring the need to better understand its role in disease progression.

Epigenetic alterations have emerged as a fundamental hallmark of cancer that drive tumorigenesis by altering cell fate decisions and differentiation (24). For example, genetic lesions involv-

Authorship note: LC and BW contributed equally to this work. WSJ is a Visiting Scholar in the Resar laboratory from the Department of Pathology, Daegu Catholic University School of Medicine, Daegu, South Korea.

Conflict of interest: The authors have declared that no conflict of interest exists.

Copyright: © 2023, Chia et al. This is an open access article published under the terms of the Creative Commons Attribution 4.0 International License.

Submitted: May 28, 2021; **Accepted:** January 25, 2023; **Published:** March 15, 2023.

Reference information: *J Clin Invest.* 2023;133(6):e151601.

<https://doi.org/10.1172/JCI151601>.

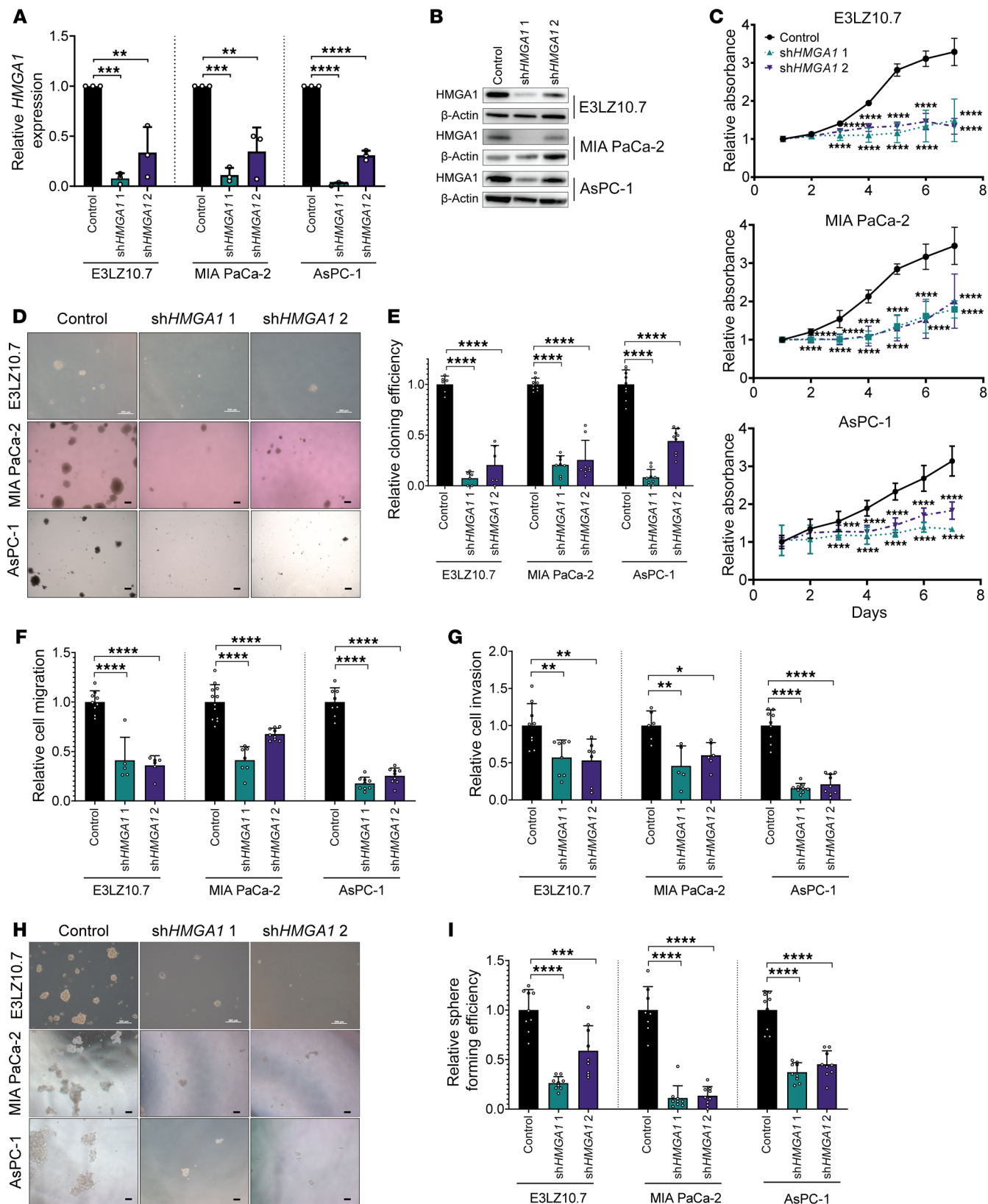


Figure 1. HMGA1 knockdown disrupts oncogenic properties in PDAC cell lines. (A) *HMGA1* expression in PDAC cell lines (E3LZ10.7, MIA PaCa-2, AsPC-1) comparing controls (transduced with empty lentiviral vector) to *HMGA1* silencing via lentiviral delivery of shRNA targeting 2 different sequences (sh*HMGA1*1, sh*HMGA1*2) from 3 experiments performed in triplicate. (B) Representative immunoblots ($n = 3$ experiments) of *HMGA1* in PDAC cells with and without *HMGA1* silencing. (C) Proliferation (by MTT) comparing PDAC cells with and without *HMGA1* silencing from 3 experiments performed in triplicate. (D) Representative images of soft agar clonogenicity assay in PDAC cells with and without *HMGA1* silencing (E3LZ10.7, $n = 2$; MIA PaCa-2 and AsPC-1, $n = 3$). Scale bars: 200 μm . (E) Clonogenic efficiency comparing PDAC cell lines with and without *HMGA1* silencing from experiments performed in triplicate (E3LZ10.7, $n = 2$; MIA PaCa-2 and AsPC-1, $n = 3$). (F) Migration comparing PDAC cells with and without *HMGA1* silencing following treatment with 10 μM cytosine β -D-arabinoside (AraC) for 1 hour to mitigate effects of proliferation from experiments performed in triplicate (E3LZ10.7 and MIA PaCa-2, $n = 2$; AsPC-1, $n = 3$). (G) Invasion comparing PDAC cells with and without *HMGA1* silencing following treatment with 10 μM AraC for 1 hour to mitigate effects of proliferation from experiments performed in triplicate (MIA PaCa-2, $n = 2$; E3LZ10.7 and AsPC-1, $n = 3$). (H) Representative images ($n = 3$ experiments) of 3D sphere formation in PDAC cell lines with and without *HMGA1* silencing. Scale bars: 200 μm . (I) 3D sphere formation comparing PDAC cell lines with and without *HMGA1* silencing from 3 experiments performed in triplicate. Data are presented as mean \pm standard deviation (SD). * $P < 0.05$, ** $P < 0.01$, *** $P < 0.001$, **** $P < 0.0001$ by 1-way ANOVA with Dunnett's multiple-comparison test (A, C, E–G, and I). Scale bars: 200 μm .

ing the switch/sucrose nonfermentable (SWI/SNF) nucleosome remodeling complex occur in up to 15% of PDAC (25). Mutations affecting histone methyltransferase genes (mixed-lineage leukemia 2 and 3) and the gene encoding the histone demethylase lysine demethylase 6A (*KDM6A*), also arise in PDAC (25). Accordingly, aberrant methylation patterns are characteristic of PDAC (26–28). Genetic alterations that decrease sirtuin 6 (*SIRT6*) protein levels, a nutrient sensor and histone deacetylase that removes acetyl groups from histone 3 lysine 9 (H3K9) and histone 3 lysine 56 (H3K56), drive pancreatic tumorigenesis in murine models and predict a subclass of human PDAC with decreased survival (29). Although these discoveries shed light on epigenetic abnormalities in PDAC, they have not led to better therapies.

Overexpression of the gene encoding the chromatin regulator *HMGA1* occurs in most aggressive tumors, including PDAC, where high levels portend poor differentiation and adverse outcomes (30–50). The *HMGA1* gene is normally expressed during embryogenesis (30, 39, 51) and in adult stem cells (46, 49, 52), but silenced postnatally in most differentiated cells. Through alternatively spliced mRNA, *HMGA1* encodes *HMGA1a* and *HMGA1b* isoforms, which bind to AT-rich sequences, bend chromatin, and recruit transcriptional complexes to modulate gene expression (31–35, 37, 39, 42, 45–47, 49, 53). When overexpressed in lymphoid cells of transgenic mice, *Hmga1* induces aggressive leukemia by upregulating transcriptional networks active in proliferating stem cells, poorly differentiated cancer cells, and inflammation (32, 35, 43, 47, 53). While mechanisms driving *HMGA1* expression in cancer are incompletely understood, growth factors (54, 55), cancer-associated mutations, including *Kras* (56) or mutant *Apc* (57), and oncogenic transcription factors, such as *cMYC* (58–60), upregulate *HMGA1*, suggesting that diverse oncogenic pathways converge on *HMGA1* to induce its expression. *HMGA1* also cooperates with

KRAS in immortalized pancreatic ductal epithelial cells to foster clonogenicity (61), whereas silencing *HMGA1* in PDAC cell lines disrupts metastatic progression following orthotopic implantation in immunodeficient mice (62). In intestinal stem cells, *HMGA1* amplifies Wnt signals from the stroma and epithelial niches by inducing the expression of genes encoding Wnt agonist receptors (*Fzd5/7*, *Lrp5/6*, and *Lgr5*) and Wnt effectors, such as *cMyc* and *Sox9* (46). Together, these findings suggest that *HMGA1* fosters tumor progression through both cell-intrinsic and stromal interactions, though little is known about transcriptional networks and tumor-stroma crosstalk governed by *HMGA1* in PDAC.

Here, we uncover what we believe is a previously unknown epigenetic program whereby *HMGA1* upregulates transcriptional networks involved in proliferation and tumor-stroma interactions during tumor progression and development of a fibroblastic stroma in PDAC. *HMGA1* binds directly to the fibroblast growth factor 19 (*FGF19*) promoter and recruits active histone marks to induce *FGF19* expression and secretion from PDAC cells. Silencing either *HMGA1* or *FGF19* disrupts phenotypes required for tumor progression. Surprisingly, loss of just a single *Hmga1* allele within the pancreatic ductal epithelium significantly prolongs survival in *Kras^{+/LSL-G12D}; Trp53^{+LSL-R172H}; Pdx1-Cre* (KPC) (63) mice compared with those with both *Hmga1* alleles intact. In mice with human PDAC xenografts, silencing *HMGA1* or *FGF19* depletes tumor-initiating cells while disrupting tumor growth and stroma formation. Moreover, treatment with an FGF receptor 4 (*FGFR4*) inhibitor, BLU9931, to block *FGF19* function (64) recapitulates the effects of *HMGA1* or *FGF19* silencing, decreasing tumor growth and stroma formation in orthotopic models. Importantly, high expression of both *HMGA1* and *FGF19* defines a subclass of human PDAC with exceptionally poor outcomes. Together, our findings reveal a unique role for *HMGA1* in tumor progression and “building” a stromal wall through *FGF19* and highlight a new therapeutic target for a subset of highly recalcitrant tumors.

Results

Silencing HMGA1 disrupts oncogenic properties and depletes tumor-initiating cells. Because *HMGA1* is upregulated in PDACs where high levels associate with decreased survival (36, 38, 61, 62), we sought to elucidate *HMGA1* function in pancreatic carcinogenesis. First, we found that *HMGA1* expression (mRNA and protein) is higher in PDAC cell lines derived from metastatic tumors compared with those from primary tumors (65) (Supplemental Figure 1, A–E; supplemental material available online with this article; <https://doi.org/10.1172/JCI151601DS1>). Next, we silenced *HMGA1* via lentiviral delivery of short hairpin RNAs (shRNAs) targeting 2 different sequences (49) in cell lines from primary and metastatic tumors harboring common PDAC mutations: (a) E3LZ10.7 (66), from a liver metastasis with *KRAS^{G12D}* and homozygous *SMAD4* deletion; (b) MIA PaCa-2 (67), from a primary PDAC with homozygous *CDKN2A/p16^{INK4A}* deletion, mutant *KRAS^{G12C}*, and *TP53*; and (c) AsPC-1 (67), from PDAC ascites fluid with homozygous mutations in *KRAS^{G12D}*, *TP53^{C135fs*35}*, and *CDKN2A^{L78fs*41}*. Strikingly, *HMGA1* deficiency disrupted proliferation, clonogenicity, migration, invasion, and 3-dimensional (3D) sphere formation in all cell lines tested (Figure 1), indicating that *HMGA1* is required for these oncogenic properties.

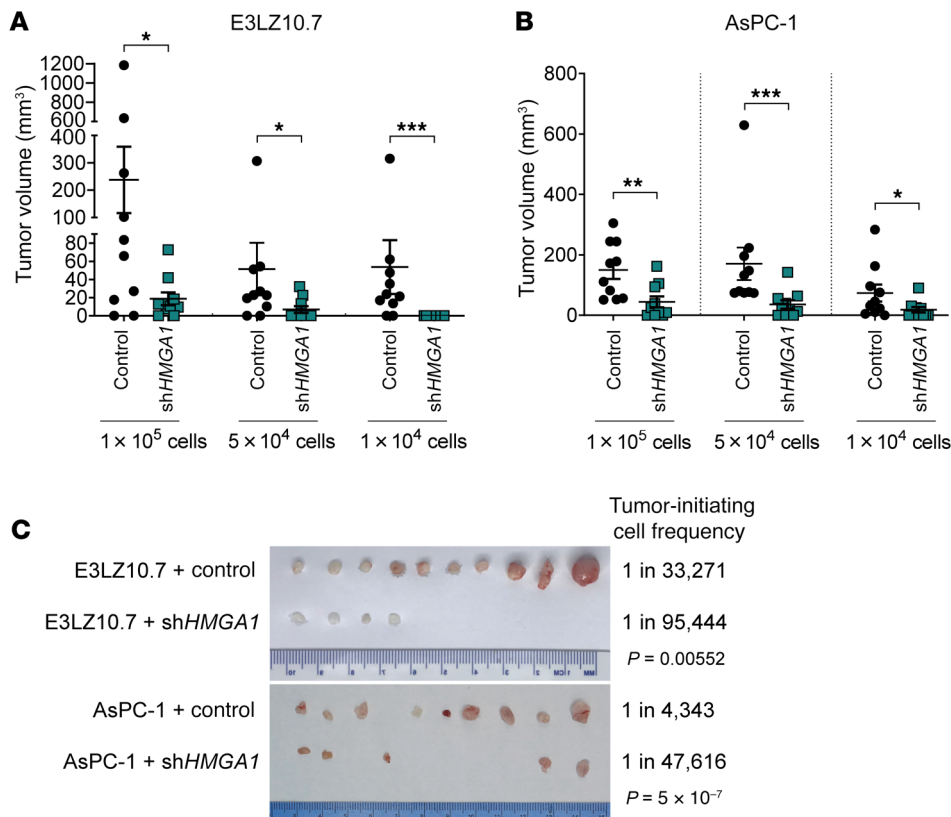


Figure 2. HMGA1 knockdown disrupts tumorigenesis and depletes tumor-initiating cells. (A) Xenograft tumorigenicity at limiting dilutions comparing E3LZ10.7 cell HMGA1 silencing ($n = 10/\text{condition}$). (B) Xenograft tumorigenicity at limiting dilutions comparing AsPC-1 cells with and without HMGA1 silencing ($n = 10/\text{condition}$). (C) Comparison of tumors dissected at the completion of experiment with 1×10^4 PDAC cells with and without HMGA1 silencing (left) and calculated frequency of tumor-initiating cells (right) in PDAC cells (E3LZ10.7, AsPC-1) with and without HMGA1 silencing. Tumor-initiating cell frequency was calculated by extreme limiting dilution analysis (ELDA; ref. 102). Data shown as mean \pm standard error of the mean (SEM). * $P < 0.05$, ** $P < 0.01$, *** $P < 0.001$ by Mann-Whitney test (A and B) or χ^2 test (C).

To define HMGA1 function in vivo, we assessed xenograft tumorigenesis from PDAC cell lines (E3LZ10.7 and AsPC-1), which showed that HMGA1 deficiency decreases tumor volumes (Figure 2, A and B). Intriguingly, tumors that formed from the pool of cells with HMGA1 silencing (E3LZ10.7 and AsPC-1 cells) express higher HMGA1 than the injected cells, suggesting that escape from gene silencing and a specific level of HMGA1 is required for tumor formation (Supplemental Figure 1, F and G). HMGA1 deficiency also depletes tumor-initiating cells in both cell lines (E3LZ10.7 and AsPC-1), demonstrating that HMGA1 is required for tumor initiation and growth in xenograft models (Figure 2C and Supplemental Figure 1, H and I).

HMGA1 regulates transcriptional networks involved in proliferation and signaling. To identify HMGA1 transcriptional networks, we performed RNA sequencing (GSE222890) in E3LZ10.7 cells (Figure 3, A and B) with or without HMGA1 silencing. Unsupervised hierarchical clustering separated cells with high HMGA1 (controls) from those with HMGA1 silencing (Supplemental Figure 2A). Differentially expressed genes ($P < 0.05$, $\log_2[\text{fold change}] > 1.5$) (68) included 660 up- and 565 downregulated genes (Figure 3B). Gene set enrichment analysis (GSEA, MSigDb Hallmark gene sets) revealed an HMGA1 signature of genes involved in cell cycle progression (E2F targets, G₂/M checkpoint, mitotic spindle genes) (Figure 3C), while curated gene sets showed enrichment for cell cycle progression, cell signaling, metastatic progression, cancer stem cells, and embryonic stem cells (Supplemental Table 1) (69, 70). Unexpectedly, we identified gene sets associated with bile acid metabolism, a pathway regulated, in part, by FGF19. Intriguingly, FGF19 (Figure 3B) was among the genes most robust-

ly upregulated by HMGA1, with greater than 20-fold differential expression. Given this robust upregulation and because growth factors can function in cell-autonomous and tumor-stroma interactions, we focused on FGF19 first. In other contexts, FGF19 promotes proliferation, and Fgf15, the murine homolog, induces hepatocellular carcinogenesis and fibrosis in mice (71–74). Further, clinical inhibitors are available to target FGF19 or its receptor, FGFR4 (64, 75–77), although the role of FGF19 in pancreatic carcinogenesis is unknown.

HMGA1 induces FGF19 expression and secretion. HMGA1-dependent expression of FGF19 (mRNA, protein) was validated in PDAC cell lines (E3LZ10.7, MIA PaCa-2, and AsPC-1; Figure 3, D and E). Intriguingly, FGF19 levels were much higher in the metastatic cell lines (E3LZ10.7 and AsPC-1) compared with MIA PaCa-2 cells derived from a localized tumor (Supplemental Figure 2B). Because FGF19 protein was barely detectable in MIA PaCa-2 cells, we validated its HMGA1 dependence by immunoprecipitation (IP) (Supplemental Figure 2C). Because FGF19 is secreted from cells and could function in an autocrine and/or paracrine fashion, we assessed secretion from E3LZ10.7 cells by cytokine arrays, which show a marked decrease with HMGA1 silencing (Figure 3, F and G); these results were validated by immunoblotting and ELISA of media (Figure 3, Hand I). Six additional secreted factors were repressed with HMGA1 silencing, 7 were increased, and 9 were unchanged (Supplemental Figure 2, D–F). Similar to the gene expression results, secreted FGF19 was among the most robustly repressed factors with HMGA1 deficiency. FGF19 secretion from AsPC-1 or MIA-PaCa-2 cells also decreased with HMGA1 silencing, as detected by ELISA of media

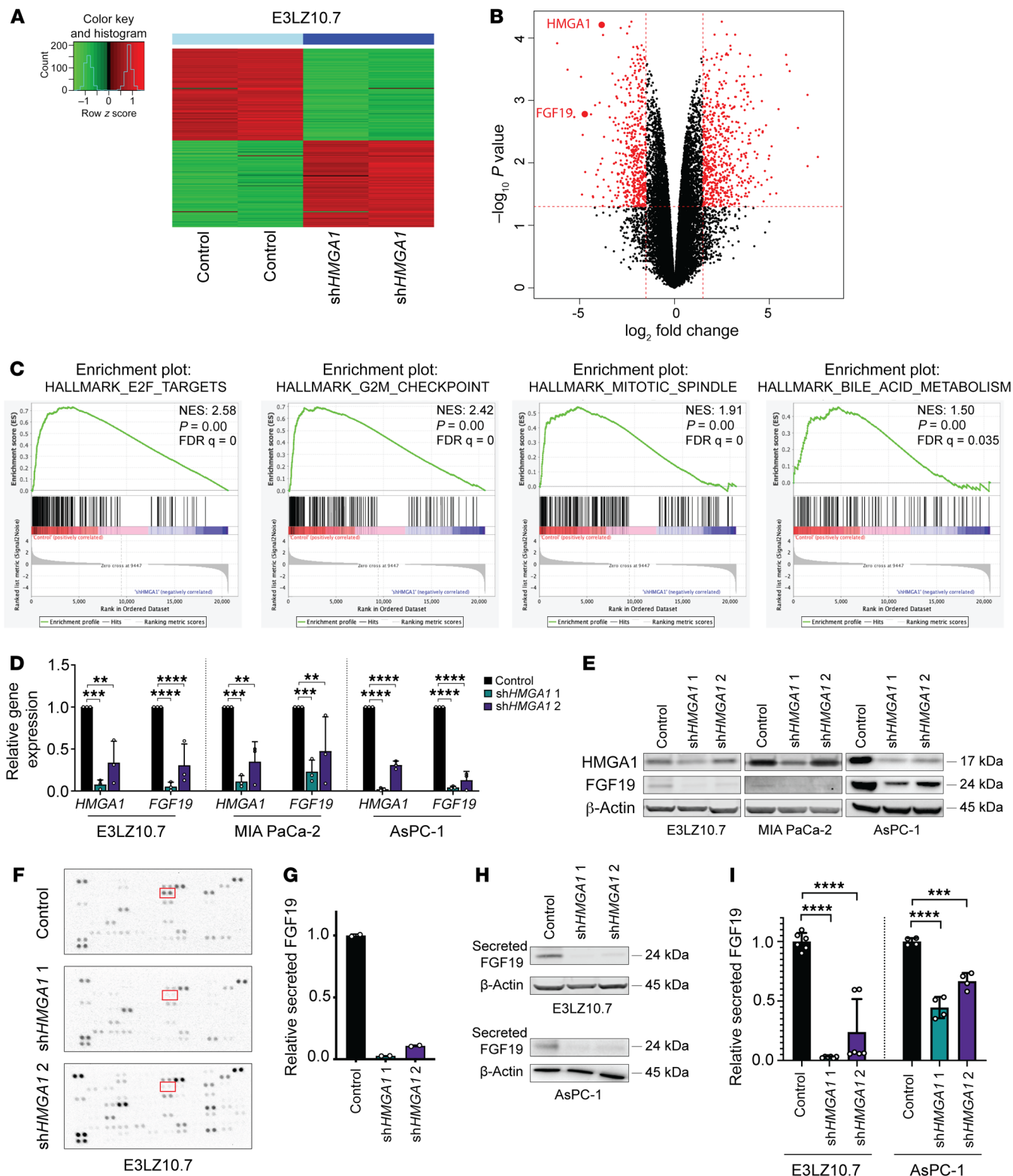


Figure 3. HMGA1 induces FGF19 expression and secretion in PDAC cell lines. (A) Heatmap from hierarchical, supervised clustering of differentially expressed genes (DEGs) comparing control E3LZ10.7 cells to those with *HMGA1* silencing (performed in duplicate in 1 RNA sequencing experiment). (B) Volcano plot of DEGs in E3LZ10.7 with and without *HMGA1* silencing reveals *FGF19* among the genes most repressed with *HMGA1* silencing. Thresholds are shown as dashed red lines; genes (dots) with significant differential expression are shown in red. $P < 0.05$, $\log_2(\text{fold change}) > 1.5$. (C) GSEA of DEGs induced by *HMGA1* in E3LZ10.7 controls (high *HMGA1*) compared to those with *HMGA1* silencing show enrichment for gene sets associated with proliferation (E2F targets, G_2/M checkpoint, mitotic spindle) and bile acid metabolism (MSigDb Hallmark). Normalized enrichment score (NES), false discovery rate (FDR), and P values are shown. (D) *FGF19* expression in PDAC cells (E3LZ10.7, MIA PaCa-2, AsPC-1) with and without *HMGA1* silencing from 3 experiments performed in triplicate. (E) Representative immunoblots ($n = 3$ experiments) of FGF19 levels in PDAC cells with and without *HMGA1* silencing. (F) Cytokine arrays of secreted protein in E3LZ10.7 cells when *HMGA1* is silenced. (G) Secreted FGF19 (relative pixel density) of duplicate spots on a single cytokine array per condition (control versus *HMGA1* silencing via sh*HMGA1* 1 or sh*HMGA1* 2). (H) Representative immunoblots ($n = 3$ experiments) of secreted FGF19 in PDAC cells (E3LZ10.7, AsPC-1) with and without *HMGA1* silencing. (I) Secreted FGF19 comparing PDAC cells (E3LZ10.7, AsPC-1) with and without *HMGA1* silencing by ELISA from experiments performed in duplicate (E3LZ10.7, $n = 3$; AsPC-1, $n = 2$). Data are presented as mean \pm SD. $**P < 0.01$, $***P < 0.001$, $****P < 0.0001$ by 1-way ANOVA with Dunnett's multiple-comparison test (D and I).

(Figure 3I and Supplemental Figure 2G). Together, these results demonstrate that FGF19 gene expression, protein levels within PDAC cells, and secretion depend upon HMGA1 in E3LZ10.7, MIA PaCa-2, and AsPC-1 cell lines.

Silencing FGF19 recapitulates effects of silencing HMGA1. To determine whether FGF19 is required for HMGA1 function in PDAC, we silenced *FGF19* in PDAC cell lines (E3LZ10.7, MIA PaCa-2, and AsPC-1) via lentiviral delivery of shRNAs targeting 2 different sequences (Figure 4, A and B, and Supplemental Figure 3A). Surprisingly, silencing *FGF19* faithfully recapitulated phenotypes observed with HMGA1 deficiency, disrupting proliferation, colony formation, migration, invasion, and 3D sphere formation (Figure 4, C–I). As an alternative approach to inhibit FGF19, we tested BLU9931, an inhibitor that specifically blocks the canonical FGF19 receptor (FGFR4) (64), demonstrating that BLU9931 impairs the proliferation, migration, and invasiveness of PDAC cell lines (E3LZ10.7 and MIA PaCa-2; Supplemental Figure 3, B–D). In xenograft tumorigenesis with E3LZ10.7 and AsPC-1 cells, both of which express higher levels of FGF19, the knockdown of *FGF19* decreased tumor volumes and tumor-initiating cells (Figure 5, A–C, and Supplemental Figure 3, E and F). Intriguingly, in *FGF19*-silenced tumors, one E3LZ10.7 tumor at each dilution and one AsPC-1 tumor at the lowest dilution grew to proportions equal to or greater than controls. We therefore reassessed *FGF19* levels in these tumors and noted a marked increase in *FGF19* relative to the injected pool, suggesting that escape from *FGF19* silencing allowed enhanced tumor growth (Supplemental Figure 3, G and H).

To determine whether exogenous FGF19 could rescue the effects of *HMGA1* silencing, we exposed PDAC cells with *HMGA1* silencing (E3LZ10.7) to recombinant human FGF19 (hFGF19). Proliferation (via 5-ethynyl-2'-deoxyuridine [EdU] incorporation)

increased upon treatment with hFGF19, but not to levels of the control cells (Supplemental Figure 3I), indicating that FGF19 is required, but not sufficient, for proliferation mediated by HMGA1. Together, our results indicate that *FGF19* is a partial mediator of HMGA1 oncogenic function in these PDAC models.

HMGA1 binds directly to the FGF19 promoter and recruits activating histone marks. Using an in silico prediction algorithm (MatInspector) (78), we identified putative HMGA1 DNA binding sites within the *FGF19* promoter at -1092 , -832 , and -810 base pairs (designated sites A, B, and C, respectively) upstream of the transcription start site (TSS) (Figure 6A). HMGA1 occupancy by chromatin IP-PCR (ChIP-PCR) demonstrated that regions (~ 200 base pairs) surrounding site A (region 1, R1) or the region encompassing sites B and C (R2) show enrichment for HMGA in cell lines (E3LZ10.7, MIA PaCa-2, and AsPC-1), which was depleted with *HMGA1* knockdown (Figure 6, B–D). The positive control, histone H3, was unchanged with HMGA1 deficiency. By contrast, there was no significant occupancy, nor were there changes with HMGA1 deficiency using a negative control IgG antibody (Figure 6E).

Because our gene expression data show that HMGA1 induces *FGF19*, we assessed occupancy of active histone H3 lysine 4 trimethylation (H3K4me3) and histone H3 lysine 27 acetylation (H3K27Ac), both of which mark promoter and enhancer regions. In 3 cell lines (E3LZ10.7, MIA PaCa-2, and AsPC-1), H3K4me3 was abundant at R1 and R2 and decreased with *HMGA1* silencing (Figure 6, E–G). HMGA1 deficiency also depleted H3K4me3 at R1 in AsPC-1 cells (Figure 6G). These data indicate that HMGA1 binds directly to the *FGF19* promoter at R1 and R2 and recruits H3K4me3 in all 3 PDAC cell lines. In the metastatic E3LZ10.7 and AsPC-1 cell lines, HMGA1 also recruited H3K27Ac to R2. Of note, H3K27Ac histone marks associate with poised chromatin, stretch, or “super-enhancers,” and regulation of developmental or stem cell-like genes during normal development and in cancer (79). Poised enhancers at developmental promoters are also implicated in poorly differentiated cancers and cancer stem cells (80). Although there are differences in the specific histone marks between cell lines, HMGA1 was consistently associated with occupancy of active histone marks at the *FGF19* promoter in all 3 cell lines.

To functionally validate these chromatin marks, we determined whether HMGA1 transactivates the *FGF19* promoter linked to a luciferase reporter gene. We tested a promoter construct (-1144) including regions R1, R2, and downstream sequences up to the TSS compared with constructs with 5' deletions: (a) -1046 , lacking R1 and site A; (b) -816 , lacking R1, site A, 5' sequences of R2, and site B; and (c) -756 , lacking R1, R2, and sites A, B, and C. As expected, the -1144 construct showed the greatest reporter activation, with decreases in constructs -816 and -756 , and the lowest activity in the construct lacking both R1 and R2 (Figure 7A). Promoter activity of the full-length construct also decreases to levels of the deletion constructs in the presence of either a dominant-negative HMGA1 that no longer binds to DNA (81) or with *HMGA1* silencing (Figure 7, B and C). These findings indicate that HMGA1 directly transactivates *FGF19* expression by binding to R1 and R2 and recruiting active histone marks.

HMGA1 signals through FGF19/FGFR4. To determine whether HMGA1 and FGF19 signal through FGFR4, we assessed phos-

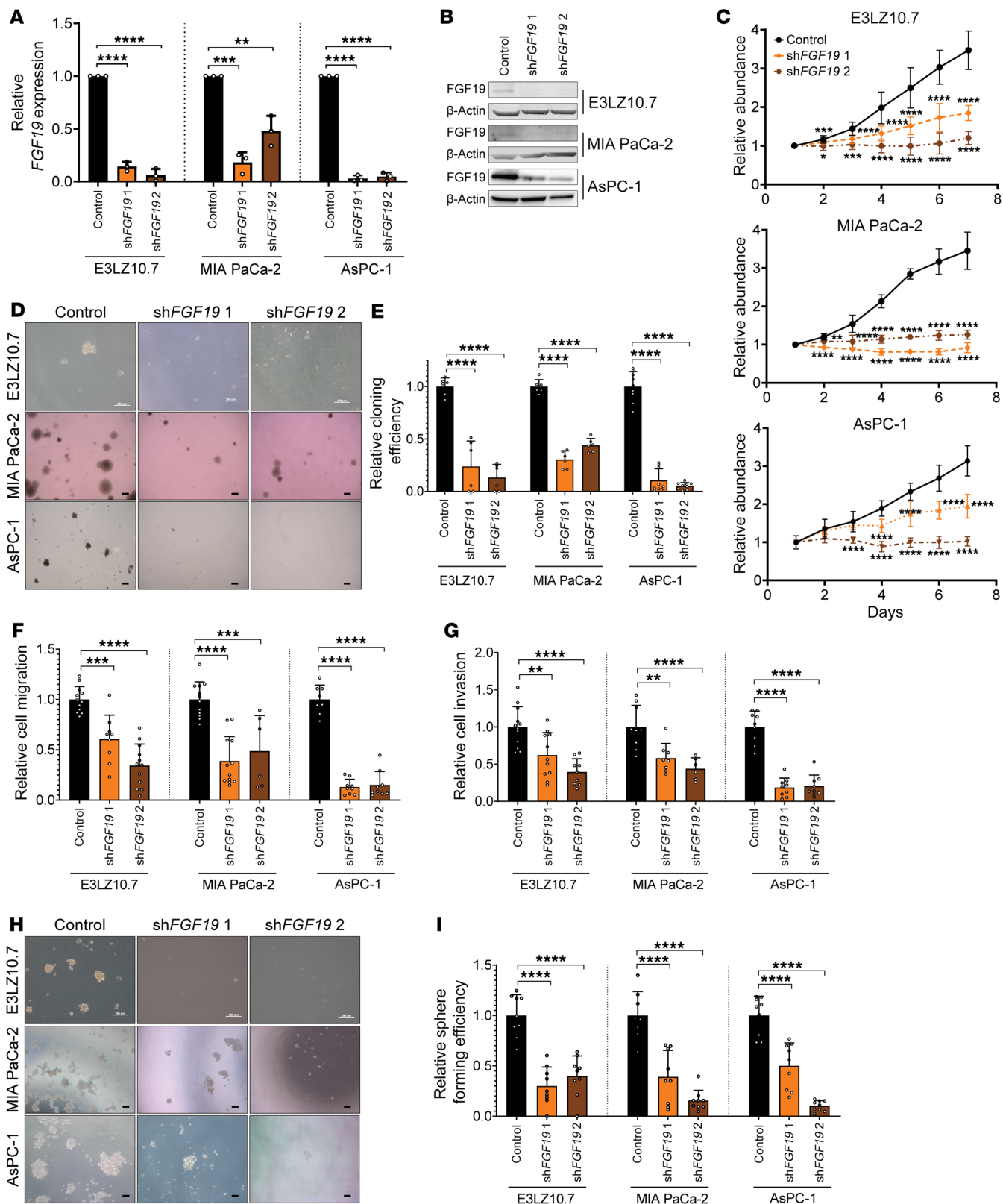


Figure 4. *FGF19* knockdown recapitulates most phenotypes associated with *HMGA1* deficiency in PDAC cell lines. (A) *FGF19* expression in PDAC cells (E3LZ10.7, MIA PaCa-2, AsPC-1) comparing controls (empty lentiviral vector) to those with *FGF19* silencing via lentiviral delivery of shRNA targeting 2 different sequences (sh*FGF19* 1, sh*FGF19* 2) from 3 experiments performed in triplicate. (B) Representative immunoblots ($n = 3$ experiments) of FGF19 protein levels in PDAC cells with and without *FGF19* silencing. (C) MTT proliferation assays comparing PDAC cells with and without *FGF19* silencing from 2 experiments performed in triplicate. (D) Representative images of clonogenicity assay comparing PDAC cells with and without *FGF19* silencing (E3LZ10.7, MIA PaCa-2, $n = 2$; AsPC-1, $n = 3$). Scale bars: 200 μm . (E) Clonogenic efficiency comparing PDAC cell lines with and without *HMGA1* silencing from experiments performed in triplicate (E3LZ10.7, MIA PaCa-2, $n = 2$; AsPC-1, $n = 3$). (F) Migration assay comparing PDAC cells with and without *FGF19* silencing following treatment with 10 μM β -D-arabinoside (AraC) for 1 hour to mitigate effects of proliferation silencing from experiments performed in triplicate (MIA PaCa-2, $n = 2$; E3LZ10.7, AsPC-1, $n = 3$). (G) Invasion assay comparing PDAC cells with and without *FGF19* silencing following treatment with 10 μM AraC for 1 hour to mitigate effects of proliferation silencing from experiments performed in triplicate (MIA PaCa-2, $n = 2$; E3LZ10.7, AsPC-1, $n = 3$). Scale bars: 200 μm . (H) Representative images ($n = 3$ experiments) of 3D sphere-formation assay comparing PDAC cells with and without *HMGA1* silencing. (I) 3D sphere formation comparing PDAC cell lines with and without *HMGA1* silencing from 3 experiments performed in triplicate. Data are presented as mean \pm SD. * $P < 0.05$, ** $P < 0.01$, *** $P < 0.001$, **** $P < 0.0001$ by 1-way ANOVA with Dunnett's multiple-comparison test (A, C, E-G, and I). Scale bars: 200 μm .

phorylation of FGFR4 and downstream signals (ERK and AKT) by flow cytometry and Western blotting in PDAC cells (E3LZ10.7 and AsPC-1). Silencing either *HMGA1* or *FGF19* decreased phosphorylation of FGFR4 (p-FGFR4; by flow cytometry) and downstream signaling molecules (ERK and AKT) without affecting unphosphorylated protein levels, indicating that both *HMGA1* and *FGF19* transduce signals through canonical *FGF19/FGFR4* pathways (Figure 8, A-F). After rendering cells (E3LZ10.7, MIA-PaCa-2, and AsPC-1) quiescent by serum deprivation, FGFR4 phosphorylation and proliferation increased with exposure to recombinant hFGF19 (Supplemental Figure 4, A-F). Together, these results suggest that *HMGA1* induces *FGF19* expression and protein secretion, resulting in the phosphorylation of FGFR4 and downstream signaling molecules to enhance proliferation in PDAC cells.

HMGA1 and *FGF19* associate with fibrotic stroma formation. Because secreted FGF19 could interact with stroma, we determined whether *HMGA1* or *FGF19* modulates fibrosis (via trichrome staining) and CAF composition within the stroma. Fibrosis scores were assigned based on area staining with trichrome: 0 (<5%), 1 (5%–30%), 2 (30%–60%), and 3 (>60%). In control PDAC xenografts, extensive fibrosis comprised over 30%–60% of tumor volumes (fibrosis scores 2–3) and included both stromal cells with a characteristic fibroblast appearance (Figure 9, A and B, and Supplemental Figure 5, A and B) and tumor cells with extensive intranuclear *HMGA1* staining and cytoplasmic FGF19 staining by immunohistochemistry (IHC) (Figure 9A and Supplemental Figure 5A). In contrast, xenografts from PDAC cells with *HMGA1* or *FGF19* silencing had less fibrosis (<30% area; Figure 9, A and B, and Supplemental Figure 5, A and B). Both *HMGA1* and FGF19 staining also decreased in tumors from PDAC cells with *HMGA1* silencing and *FGF19* silencing also decreased FGF19

staining (Figure 9A and Supplemental Figure 5A). Of note, tumors arising from cells with *HMGA1* knockdown included a subset of tumor cells with *HMGA1* intranuclear staining resembling controls, consistent with our gene expression data suggesting that escape from *HMGA1* silencing allows tumor cells to grow as xenografts (Supplemental Figure 1, F and G). Further, the proliferation marker Ki-67 decreased with *HMGA1* or *FGF19* silencing in PDAC xenografts (Figure 9, A and C, and Supplemental Figure 5, A and C). These findings indicate that *HMGA1* and *FGF19* promote tumor proliferation and stroma formation in xenografted tumors.

To elucidate *HMGA1*-dependent changes in CAF composition within the stroma of xenografted tumors, we performed immunofluorescence (IF) to classify CAFs into 3 major subtypes previously defined in KPC mice and human tumors (19–23) based on positive staining for podoplanin (PDPN; a pan-CAF marker) and (a) α -smooth muscle actin (α -SMA); (b) CD74, a transmembrane molecule involved in formation and transport of major histocompatibility (MCH) class II peptides; and (c) IL-6, an inflammatory cytokine. In PDAC xenografts from all 3 cell lines, α -SMA⁺ CAFs comprised the majority, with less contribution from CD74⁺ and IL-6⁺ CAFs. Silencing *HMGA1* or *FGF19* reduced the proportion of all 3 CAF subtypes (Figure 9, D and E, and Supplemental Figure 5, D and E). Together, these findings indicate that *HMGA1* and *FGF19* modulate CAF composition to induce the formation of a desmoplastic stroma in xenografted tumors.

Hmga1 deficiency in KPC mice impairs tumor and stroma formation. To investigate *Hmga1* in tumorigenesis, CAF composition, and stroma formation in mice with a competent immune system, we crossed KPC mice, in which PDAC develops more gradually (63), with mice with global deficiency of one or both *Hmga1* alleles (all on C57BL/6 backgrounds) and followed offspring for evidence of PDAC (abdominal distension, rectal prolapse, palpable tumors) or ill appearance (hunching, or decreased activity, oral intake, or weight; Table 1). Similar to prior reports (63), KPC mice (24 of 24 evaluable mice) developed pancreatic tumors by 14.1 weeks [median survival time] (Supplemental Figure 6A). Tissue autolysis precluded further analyses in 2 mice that died at 8 and 16 weeks. A subset of KPC mice developed rectal prolapse (5 of 24) and/or ascites (3 of 24) (Table 1). In all cases, invasive pancreatic tumors developed (24 of 24) with pathology consistent with PDAC in most (92%; 22 of 24); 2 developed an undifferentiated sarcomatoid pancreatic tumor. By contrast, KPC mice with *Hmga1* heterozygosity had delayed tumorigenesis and prolonged survival ($n = 9$; median survival 17.0 weeks). One KPC/*Hmga1* heterozygous mouse developed a large salivary gland tumor at 7.4 weeks of age; the pancreas showed only rare foci of acinar ductal metaplasia. Of note, *Hmga1* heterozygous mice have normal life expectancy with no evidence of abnormal growth or development (48, 49). We also generated 1 KPC mouse null for *Hmga1*, which had a normal pancreas size and only rare foci of acinar ductal metaplasia at 22 weeks; it was sacrificed prior to any evidence of illness. *Hmga1*-knockout mice have decreased embryonic viability, whereas those that survive development are slightly small but appear grossly normal up to 30 weeks of age when they develop signs of premature aging (graying, osteopenia, decreased gait velocity) (49). We used ultrasound to confirm the presence of pancreatic tumors in a subset of mice (Supplemental Figure 6B).

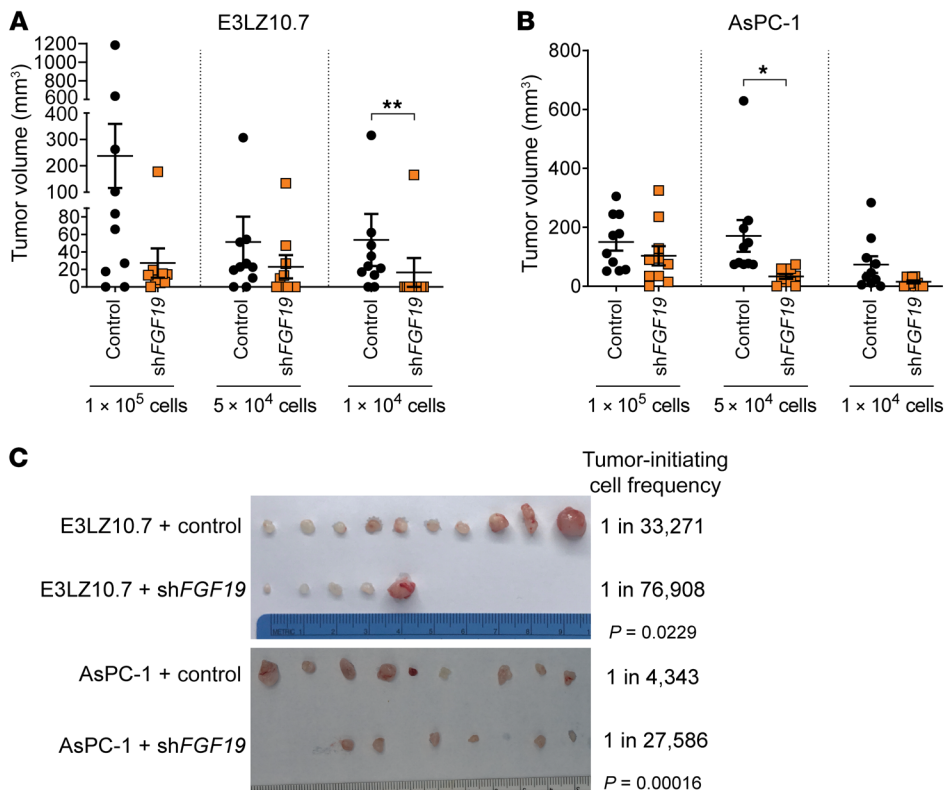


Figure 5. FGF19 knockdown disrupts tumorigenesis and depletes tumor-initiating cells, similar to phenotypes observed with HMGA1 silencing in PDAC xenografts. (A) Xenograft tumorigenicity at limiting dilutions comparing E3LZ10.7 cells with and without FGF19 silencing ($n = 10$ /condition). (B) Xenograft tumorigenicity at limiting dilutions comparing AsPC-1 cells with and without FGF19 silencing ($n = 10$ /condition). (C) Comparison of tumors dissected at the completion of experiment with 1×10^4 PDAC cells (E3LZ10.7, AsPC-1) with and without FGF19 silencing (left) and calculated frequency of tumor-initiating cells (right) among PDAC cells. Tumor-initiating cell frequency calculated by ELDA (102). Data shown as mean \pm SEM. * $P < 0.05$, ** $P < 0.01$ by Mann-Whitney test (A and B) or χ^2 test (C).

To ascertain whether *Hmga1* deficiency alters pancreatic stroma development and fibrosis in KPC mice, we validated HMGA1 deficiency (via IHC), which showed robust HMGA1 intranuclear staining in KPC mice, less staining in KPC mice with *Hmga1* heterozygosity, and complete absence of HMGA1 in KPC/*Hmga1*-knockout mice (Supplemental Figure 6C). FGF19 staining paralleled results observed with HMGA1, with robust FGF15 staining in KPC mice, moderate staining in KPC/*Hmga1* heterozygous mice, and low levels in the KPC pancreas with *Hmga1* knockout (Supplemental Figure 6C). Similarly, fibrosis scores decreased in KPC mice with a deficiency of one *Hmga1* allele (Supplemental Figure 6, C and D, and Table 1), while the *Hmga1*-knockout mouse did not develop PDAC or fibrosis by 22 weeks. These data demonstrate that HMGA1 is required for pancreatic tumorigenesis and stromal formation in KPC mice.

Hmga1 haploinsufficiency within pancreatic ductal epithelium is sufficient to mitigate tumor and stroma formation in KPC mice. To determine whether *Hmga1* deficiency within the pancreatic ductal epithelium is sufficient to mitigate tumorigenesis and stroma formation, we generated KPC mice crossed with mice with one or both *Hmga1* alleles floxed, resulting in deletion of floxed alleles within pancreatic epithelium, including KPC mice with pancreas-specific heterozygous (KPC/*Hmga1*^{f/+}) or homozygous (KPC/*Hmga1*^{f/f}) deletions. Surprisingly, loss of just a single *Hmga1* allele within the pancreas (KPC/*Hmga1*^{f/+}) was sufficient to delay tumorigenesis and prolong survival ($n = 5$; 22.3 weeks) in KPC mice, and survival was prolonged even more than what we observed for KPC mice with global *Hmga1* heterozygous deficiency (Figure 10A). Survival was also prolonged in mice with pancreas-specific deletion of both *Hmga1* alleles ($n = 7$; KPC/*Hmga1*^{f/f}; 22.0 weeks) similar to the

KPC/*Hmga1*^{f/+}, suggesting that loss of just a single *Hmga1* allele is sufficient to mitigate tumorigenesis in KPC mice. Accordingly, HMGA1 IHC in KPC/*Hmga1*^{f/+} or KPC/*Hmga1*^{f/f} mice showed a decrease or absence of HMGA1 in tumors cells, respectively, and FGF15 staining also decreased in parallel with HMGA1 (Figure 10B). Moreover, fibrosis scores and Ki-67 decreased in KPC mice with *Hmga1* deficiency within pancreatic epithelium (Figure 10, B–D). Further, all 3 major CAF subtypes (by IF) decreased with pancreatic epithelial *Hmga1* deficiency (Figure 10, E and F). Together, these striking results demonstrate that the loss of just a single *Hmga1* allele within the pancreatic ductal epithelium is sufficient to mitigate tumorigenesis, stroma formation, and modulate CAF composition, thereby prolonging survival in KPC mice.

HMGA1 and *FGF19* are upregulated in human PDAC with exceptionally poor outcomes. To determine whether *HMGA1* and *FGF19* are relevant in human PDAC, we queried published data sets (GSE15471; $n = 36$ nonmalignant tissue, $n = 36$ tumor samples) (82). As expected, *HMGA1* was robustly upregulated in most human PDACs, consistent with prior studies (Figure 11A) (36, 38). By contrast, *FGF19* was variable, with tumors demonstrating low, moderate, or high expression (Figure 11A). However, *HMGA1* and *FGF19* correlated positively in all tumors, albeit weakly (Figure 11B). In another independent data set (GSE16515) (83), we validated similar patterns with consistent *HMGA1* overexpression and a broader range of *FGF19* expression (Supplemental Figure 7D). Since *HMGA1* is overexpressed in most tumors, whereas *FGF19* is upregulated in only a subset (~25%), we determined whether high expression of both *HMGA1* and *FGF19* predicts outcomes. In a PDAC database with survival data (GSE21501; $n = 102$ PDAC tumors) (84), we categorized PDAC tumors ($n = 102$) by quartiles

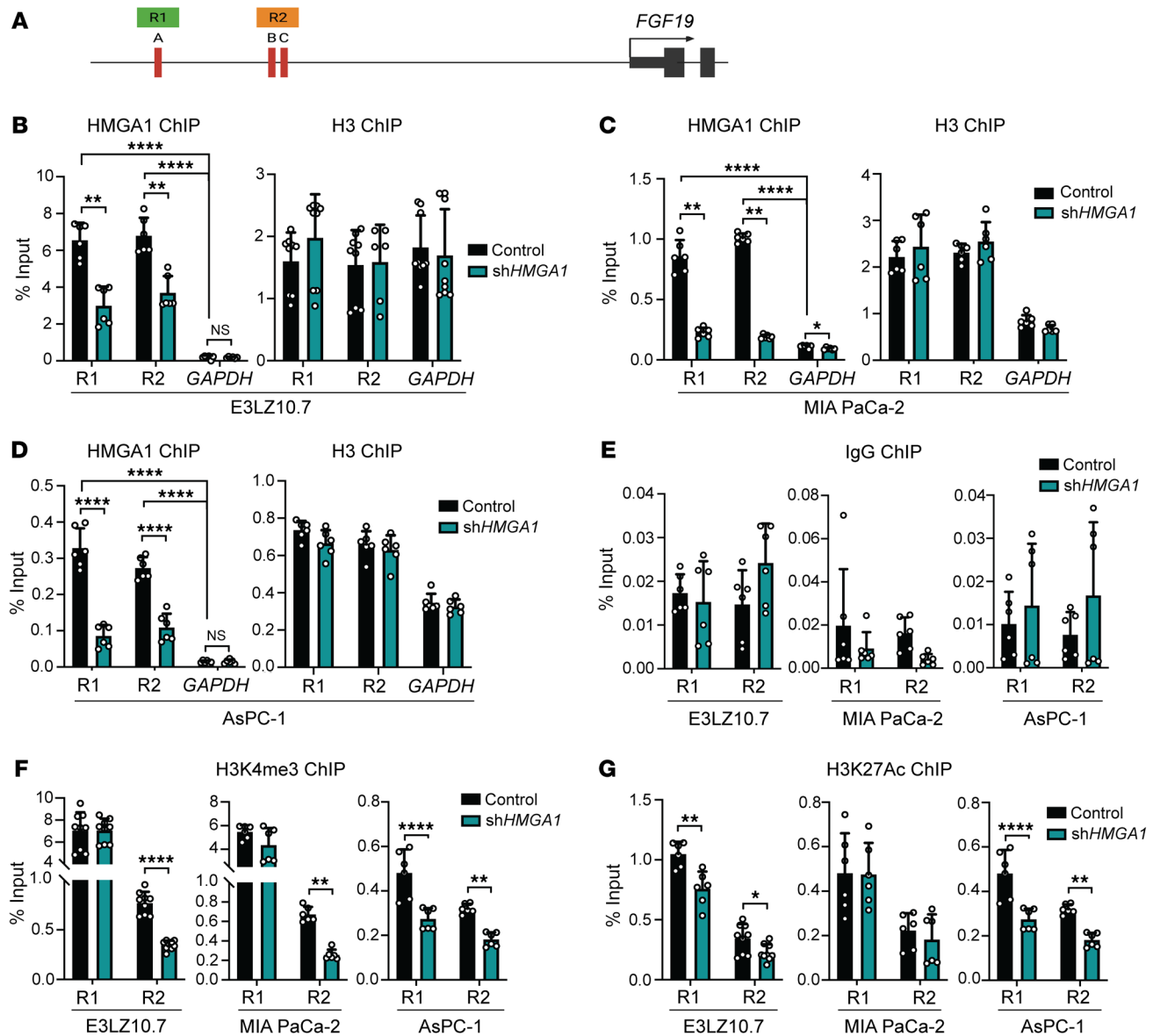


Figure 6. HMGA1 induces *FGF19* expression by binding to the *FGF19* promoter and recruiting active histone marks. (A) Schematic representation of the *FGF19* promoter; R1 includes predicted HMGA1 binding site A; R2 includes predicted HMGA1 sites B and C. (B) ChIP-PCR comparing HMGA1 occupancy on the *FGF19* promoter in E3LZ10.7 cells with and without *HMGA1* silencing. (C) ChIP-PCR comparing HMGA1 occupancy on the *FGF19* promoter in MIA PaCa-2 cells with and without *HMGA1* silencing. (D) ChIP-PCR comparing HMGA1 occupancy on the *FGF19* promoter in AsPC-1 cells with and without *HMGA1* silencing. In B–D, histone H3 served as a positive control for chromatin pull-down and the *GAPDH* promoter sequence as a negative control. (E) ChIP-PCR of control IgG at R1 and R2 in PDAC cells (E3LZ10.7, MIA PaCa-2, AsPC-1) with and without *HMGA1* silencing. (F) ChIP-PCR for the H3K4me3 active histone mark on the *FGF19* promoter in PDAC cells (E3LZ10.7, MIA PaCa-2, AsPC-1) with and without *HMGA1* silencing. (G) ChIP-PCR for the H3K27Ac active histone mark on the *FGF19* promoter in PDAC cells with and without *HMGA1* silencing. All ChIP-PCR results are shown from 2 experiments performed in triplicate. Data are presented as mean \pm SD. Significance was evaluated by 1-way ANOVA with Dunnett's multiple-comparison test (B–E), 2-tailed Student's *t* test (E3LZ10.7, AsPC-1 cells; data normally distributed) and Mann-Whitney test (MIA PaCa-2 cells; data not normally distributed) (F), or Mann-Whitney test (G). * $P < 0.05$, ** $P < 0.01$, **** $P < 0.0001$.

based on relative expression of both genes, with the upper quartile representing tumors with highest expression of *HMGA1* and *FGF19* (red line; $n = 26$) and the lower quartile representing tumors with lowest expression of *HMGA1* and *FGF19* (black line; $n = 26$). We included a quartile with high *HMGA1* and low *FGF19* (green line; $n = 25$) and relatively low *HMGA1* with high *FGF19* (blue line; $n = 25$) (Figure 11C). Strikingly, tumors with high levels of both *HMGA1* and *FGF19* had worse overall survival ($P = 0.005$), indi-

cating that this pathway is relevant to human PDAC and further underscoring *FGF19* as a plausible therapeutic target for this highly recalcitrant molecular subtype (Figure 11C).

BLU9931 decreases tumorigenesis and stroma formation in orthotopic PDAC models. Because our primary goal is to identify actionable mechanisms in PDAC, we determined whether targeting the *HMGA1/FGF19* pathway with *BLU9931* mitigates tumor and stroma formation. We tested *BLU9931* at doses established to reach

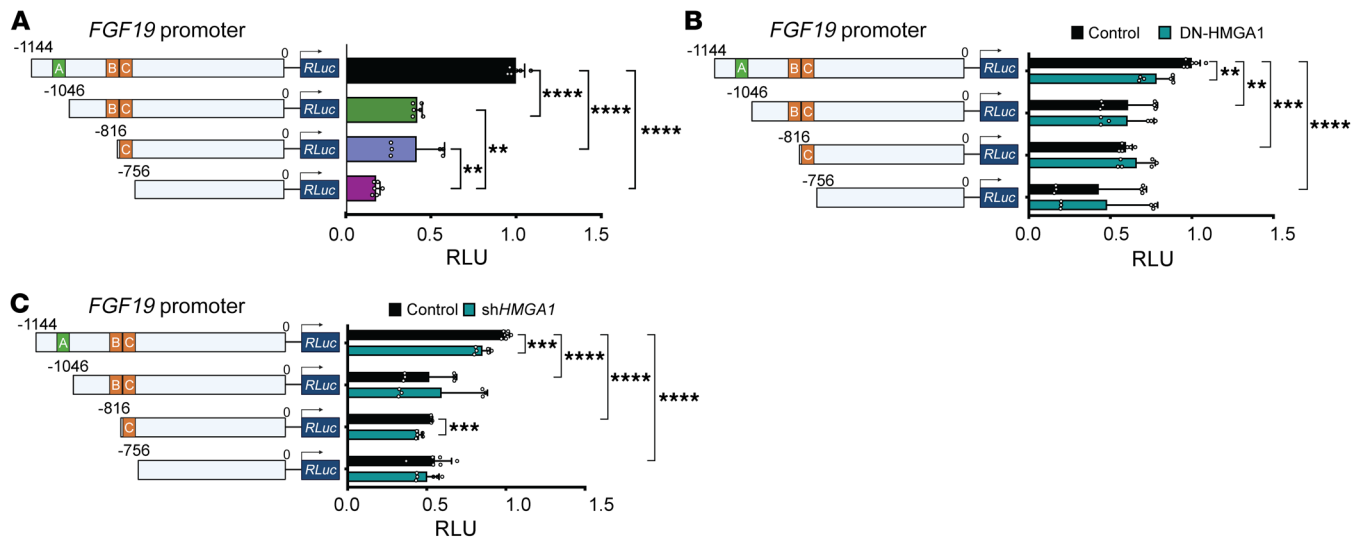


Figure 7. HMGA1 binds to the *FGF19* promoter to induce *FGF19* expression. (A) Reporter gene activity (via dual-luciferase assay) in E3L210.7 cells transfected with *FGF19* promoter constructs. (B) Reporter gene activity (via dual-luciferase assay) in E3L210.7 cells after cotransfection with dominant-negative HMGA1 or control vector and *FGF19* promoter constructs. (C) Reporter gene activity (via dual-luciferase assay) in E3L210.7 cells after cotransfection with HMGA1 silencing or control vector and *FGF19* promoter constructs. Data shown as mean \pm SD from 2 independent experiments performed in triplicate. ** $P < 0.01$, *** $P < 0.001$, **** $P < 0.0001$ by 1-way ANOVA with Dunnett's multiple-comparison test (A–C). RLU, relative luminescence units.

pharmacologic levels in mice (64) in human PDAC xenografts from E2L210.7 cells (1×10^6) injected into the midpancreas of immunosuppressed mice (NOD Scid γ , NSG). Once tumors reached a volume of 100–200 mm³ by ultrasound, mice were given BLU9931 twice daily by oral gavage (300 mg/kg or vehicle control) approximately 1 week following implantation. Mice underwent necropsy after 4 weeks of therapy when controls began to appear ill. Strikingly, there was a marked decrease in tumor volumes in mice treated with BLU9931, along with decreased staining for HMGA1, FGF19, Ki-67, and fibrosis (trichrome) (Figure 12, A–D). The 3 CAF subtypes also decreased with BLU9931 (Figure 12, E and F), suggesting that targeting FGFR4 with BLU9931 is a promising approach for human PDAC overexpressing HMGA1 and FGF19.

Next, we tested BLU9931 in syngeneic mice with an intact immune system and KPC orthotopic implants. After generating subcutaneous xenografts from KPC and KPC/*Hmga1*^{fl/+} heterozygous cell lines with tumor volumes of approximately 100–200 mm³, tumor fragments were implanted surgically into the pancreas of mice. One week after implantation, we confirmed tumor formation (volumes of 100–200 mm³) by ultrasound, after which mice were divided into treatment arms with similar tumor volume distributions ($n = 8$ –10/group): (a) KPC implants, BLU9931 treatment (twice daily oral gavage); b) KPC implants, vehicle control (twice daily oral gavage); c) KPC-*Hmga1* heterozygous implants, BLU9931 treatment; and (d) KPC-*Hmga1* heterozygous implants, vehicle control. Mice were followed by weekly ultrasounds and necropsies performed when recipients of KPC implants treated with vehicle control appeared ill (after 4 weeks). We discovered a marked decrease in tumor volume in recipients of KPC implants treated with BLU9931 compared with vehicle control (Figure 13A). Further, KPC implant recipients treated with BLU9931 had decreased levels of HMGA1, FGF19, fibrosis, and Ki-67 (Figure 13, B–D). Similar to KPC mice with *Hmga1* deficiency, the frequency of

all CAF subtypes decreased (Figure 13, E and F). Recipients of KPC implants with *Hmga1* heterozygous deficiency had slightly smaller tumors than KPC mice treated with BLU9931. Although BLU9931 resulted in slightly lower mean tumor volumes in KPC/*Hmga1* heterozygous implants in addition to decreased HMGA1, FGF15, and Ki-67 staining, and 2 of 3 CAF subtypes, the changes were modest, as tumor growth was markedly diminished by *Hmga1* haploinsufficiency alone (Supplemental Figure 8, A–E). Taken together, these results indicate that HMGA1 drives PDAC tumor initiation, progression, and stroma formation, at least in part, by inducing *FGF19* expression and secretion. Moreover, this pathway can be disrupted with an FGFR4 inhibitor, BLU9931. Most importantly, overexpression of HMGA1 and FGF19 defines a subset of human PDAC with exceptionally poor outcomes, underscoring the need for further studies to assess targeting FGF19 in PDAC.

Discussion

Alterations in chromatin regulators frequently occur in cancer, although most epigenetic modulators have eluded therapeutic targeting (85–87). For example, genes encoding chromatin regulators involved in pluripotency, *OCT4*, *SOX2*, *KLF4*, *NANOG*, and *LIN28*, are rarely mutated, but frequently overexpressed in cancer, thus rendering pharmacologic interventions challenging (87). Such factors are believed to reprogram the epigenome to a more plastic, stem-like state, thereby endowing tumor cells with the capacity to proliferate in a deregulated fashion, circumvent differentiation cues, evade therapy, and metastasize. HMGA1 chromatin regulators are oncofetal proteins that enhance cellular reprogramming by upregulating pluripotency networks (47, 88, 89). Similar to pluripotency factors, HMGA1 is rarely mutated, but almost universally overexpressed in aggressive cancers, consistent with a fundamental role in tumorigenesis (47, 88). Indeed, HMGA1 is among the most abundant, nonhistone chromatin-binding proteins with-

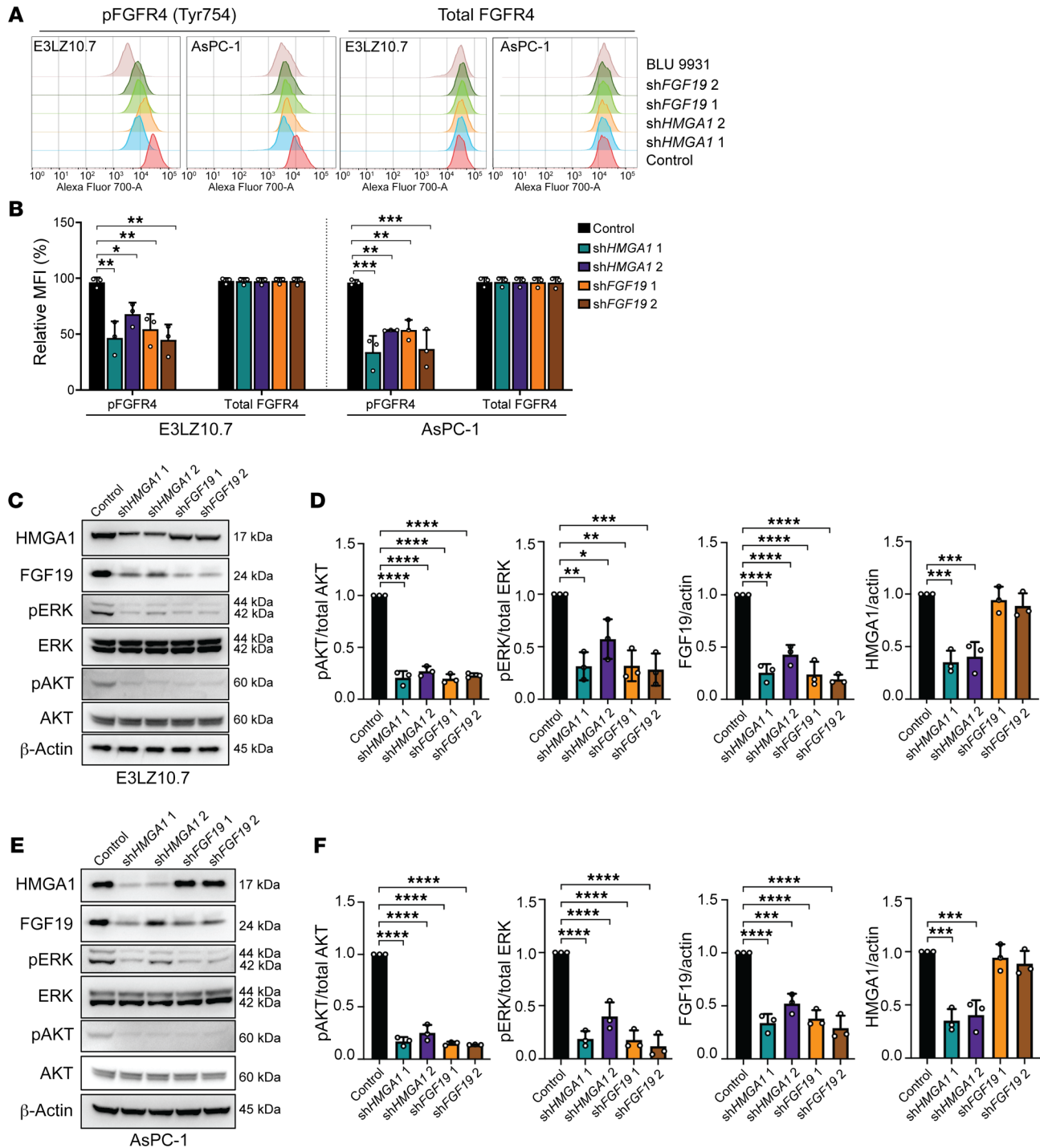


Figure 8. HMGA1 signals through the canonical FGF19/FGFR4 pathway. (A) Representative flow cytometric profiles ($n = 3$ experiments) of phosphorylated FGFR4 (p-FGFR4) and total FGFR4 in PDAC cell lines (E3LZ10.7, AsPC-1) with and without *HMGA1* silencing, *FGF19* silencing, or treatment with the FGFR4 inhibitor BLU9931 (10 μ M). (B) Comparison of mean fluorescence intensities (MFIs) of phosphorylated FGFR4 (p-FGFR4) and total FGFR4 in PDAC cell lines (E3LZ10.7, AsPC-1) with and without *HMGA1* silencing, *FGF19* silencing, or treatment with BLU9931 (10 μ M). (C) Representative immunoblots ($n = 3$ experiments) and (D) relative protein levels of FGFR4 and downstream signaling molecules (ERK, AKT), including total protein and phosphorylated proteins in E3LZ10.7 cells with and without *HMGA1* or *FGF19* silencing. (E) Representative immunoblots ($n = 3$ experiments) and (F) relative protein levels of FGFR4 and downstream signaling molecules in AsPC-1 cells with and without *HMGA1* or *FGF19* silencing. Data shown as mean \pm SD from 3 independent experiments performed in triplicate. * $P < 0.05$, ** $P < 0.01$, *** $P < 0.001$, **** $P < 0.0001$ by 1-way ANOVA with Dunnett's multiple-comparison test (B, D, and F).

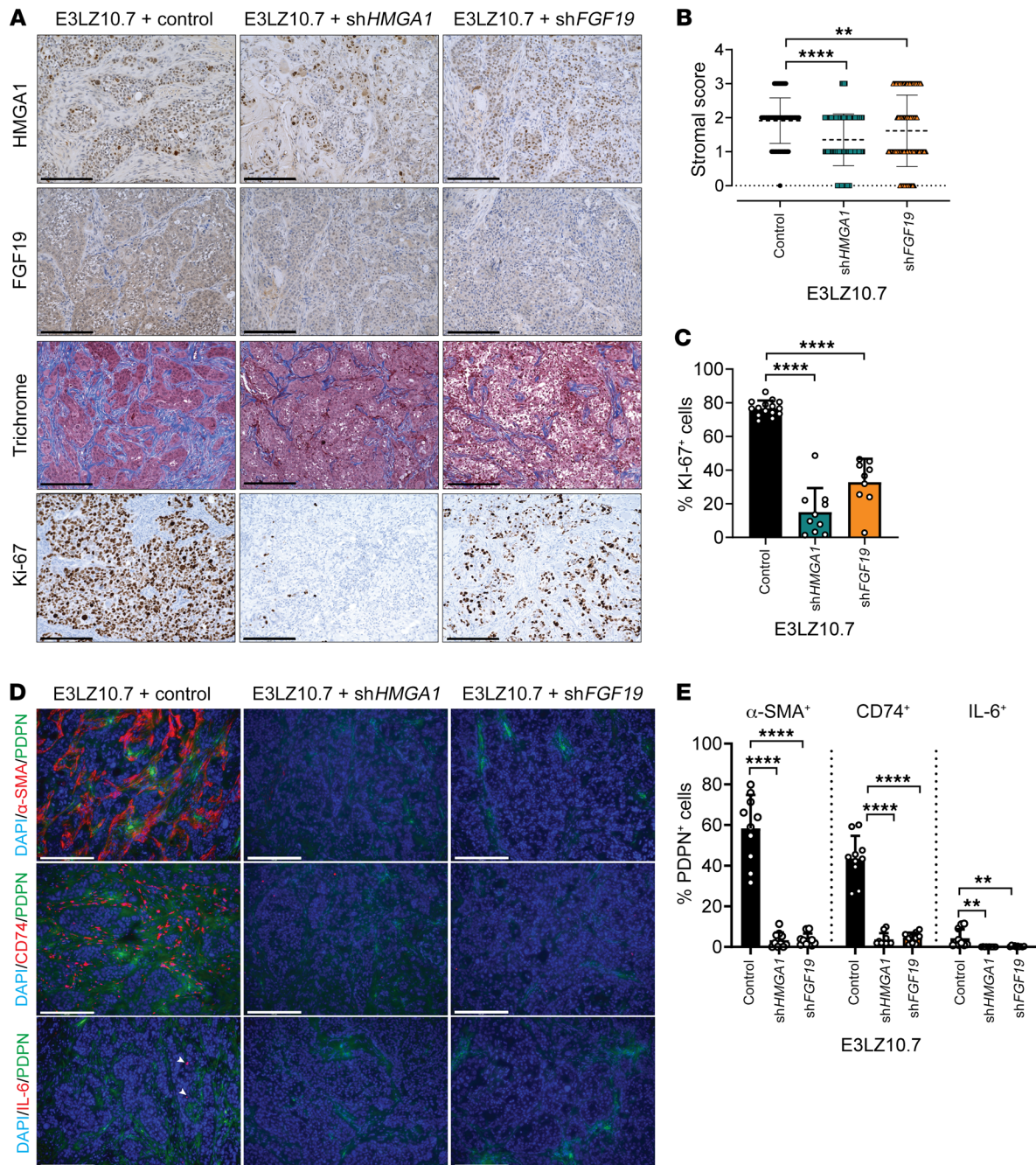


Figure 9. HMGGA1 and FGF19 induce fibrotic stroma formation, proliferation (Ki-67), and modulate CAF composition during PDAC xenograft tumorigenesis. (A) Representative images ($n = 10$ per condition) of HMGGA1 (IHC, top row), FGF19 (IHC, second row), fibrosis (trichrome, third row), and Ki-67 (IHC, bottom row) in E3LZ10.7 xenografts with and without HMGGA1 or FGF19 silencing. (B) Quantitative comparison of stroma scores in E3LZ10.7 xenografts with and without HMGGA1 or FGF19 silencing. Fibrosis scores based on 3-point system (0, <5%; 1, 5%–30%; 2, 30%–60%; 3, >60%) ($n = 16$ images taken from 3 control tumors, 2 shHMGGA1 tumors, and 4 shFGF19 tumors). (C) Comparison of Ki-67-positive cell number in xenografts (5 fields at $\times 20$ magnification of tumors from 2 different mice/group, with $n = 10$ per condition). (D) Representative IF images to compare CAF composition in E3LZ10.7 xenografts with and without HMGGA1 or FGF19 silencing. (E) Total CAF numbers were ascertained by costaining with DAPI and for PDPN; α -SMA, CD74, and IL-6 were used to identify different subtypes of CAFs. Data in D and E were based on 10 fields at $\times 20$ magnification ($n = 10$ per condition). Data presented as mean \pm SD. ** $P < 0.01$, **** $P < 0.0001$ by 1-way ANOVA with Dunnett’s multiple-comparison test (B, C, and E). Scale bars: 200 μ m.

in nuclei of cancer cells where it induces genes expressed in stem cells and tumor progression (30, 38, 46, 48, 88, 89).

While many studies show HMGGA1 upregulation in PDAC (36, 38, 50, 61), transcriptional networks governed by HMGGA1

that could be targeted in therapy remained elusive until now. We identified a single growth factor, FGF19, that fosters not only oncogenic properties, but also signals within the microenvironment to induce fibrotic desmoplasia. This mechanism is poten-

Table 1. Clinical spectrum of disease in KPC mice with and without *Hmga1*

ID	Genotype	Sex	Age (wk)	Panc weight (mg)	Panc (mg)/BW (g) ratio	PDAC	Additional histological features	Other if applicable
1	KPC	F	16	783	34.2	Y	PDAC	Rectal prolapse
2	KPC	F	13.9	1562	59.6	Y	PDAC	Hemorrhagic ascites, abdominal distension, enlarged liver and spleen, lymphoma
3	KPC	F	13.4	1031	43	Y	PDAC	Hemorrhagic ascites, abdominal distension, verrucous squamous proliferation in distal esophagus
4	KPC	F	12.7	2542	146	N	Undifferentiated, sarcomatoid	Hunched, decrease motility, cyst observed on the stomach, verrucous squamous proliferation in distal esophagus
5	KPC	F	9.6	591	28.5	Y	PDAC	Rectal prolapse, facial papilloma, hunched
6	KPC	M	15	512	25.1	Y	PDAC	Rectal prolapse, neoplasm of neuroendocrine morphology in the lungs
7	KPC	M	14	851	31.1	Y	PDAC	Facial papilloma with enlarged liver
8	KPC	F	11.4	1323	53.8	Y	PDAC	Rectal prolapse
9	KPC	F	14.3	809	24.9	Y	PDAC	Vaginal mass with facial papilloma, anal excoriation
10	KPC	M	12.9	883	30.1	Y	PDAC	Abdominal distension, decreased mobility, histiocytic sarcoma
11	KPC	F	14.1	1623	70.1	Y	PDAC	Ascites, abdominal distension, decreased mobility, cysts observed
12 ^A	KPC	F	10	1981	76.9	Y	PDAC	–
13	KPC	M	12.6	2555	94.9	Y	PDAC	Abdominal distension, palpable mass, hunching
14	KPC	M	19.5	2569	93.5	Y	PDAC	Abdominal distension, palpable mass, hunching
15	KPC	M	15.6	550	29.9	Y	PDAC	Primary lung neoplasm
16	KPC	M	15.6	449	16.9	Y	PDAC	Anal mass, additional sarcomatoid carcinoma, lymphoma(?)
17	KPC	F	15.6	1423	75.8	Y	PDAC	Abdominal distension, rectal prolapse
18	KPC	F	14	540	25.3	N	Undifferentiated, sarcomatoid	Rectal prolapse, facial papilloma, undifferentiated sarcomatoid carcinoma involving pancreas
19	KPC	M	12.1	1159	50.7	Y	PDAC	Abdominal distension, hunching, decreased mobility
20	KPC	F	13.9	725	30.9	Y	PDAC	Pancreatic tumor attached to GI tract and spleen
21 ^A	KPC	F	8.3	NA	NA	NA	Not evaluable	–
22	KPC	M	21	1141	43	Y	PDAC	–
23 ^A	KPC	F	20.9	1500	56.5	Y	PDAC	–
24	KPC	M	14.6	903	30.7	Y	PDAC	–
25	KPC	M	14.6	531	19.3	Y	PDAC	–
26 ^A	KPC	F	16	NA	NA	NA	Not evaluable	–
1	KPC/ <i>Hmga1</i> ^{-/-}	F	7.4	412	18.9	N	Generally normal pancreas with limited ADM	Salivary gland tumor
2	KPC/ <i>Hmga1</i> ^{-/-}	M	20.4	838	44.7	Y	PDAC	Rectal prolapse, cachexia, neoplasm of neuroendocrine morphology in the lungs
3	KPC/ <i>Hmga1</i> ^{-/-}	F	16.4	1645	52.9	N	ADM, PanINs, atrophic, lobular architecture present	Sarcomatoid carcinoma near the salivary glands, chronic liver hepatitis, lymphoma
4	KPC/ <i>Hmga1</i> ^{-/-}	F	13.4	2217	130	Y	PDAC	Hunched, decreased motility
5 ^A	KPC/ <i>Hmga1</i> ^{-/-}	F	23	331	23.6	Y	PDAC	Malocclusion, dehydration
6 ^A	KPC/ <i>Hmga1</i> ^{-/-}	M	17.9	781	29.7	N	Focal ADM	Decrease mobility, T cell lymphoma present
7	KPC/ <i>Hmga1</i> ^{-/-}	M	10.4	666	23.2	N	PanIN only	Myeloid sarcoma
8	KPC/ <i>Hmga1</i> ^{-/-}	F	21.85	651	NA	Y	PDAC	Abdominal distension, cyst on gall bladder, rectal prolapse, decreased motility, micrometastasis to lymph nodes
9	KPC/ <i>Hmga1</i> ^{-/-}	F	17	152	5.3	N	Generally normal pancreas	Rectal prolapse, ulceration
10	KPC/ <i>Hmga1</i> ^{fl/fl}	M	22.3	1255	58.8	Y	PDAC	Decreased mobility, palpable mass, abdominal distension, hemorrhagic ascites, eye tag
11	KPC/ <i>Hmga1</i> ^{fl/fl}	M	33.4	1827	68.8	Y	PDAC	Decreased mobility, hemorrhagic ascites, hunching
12 ^A	KPC/ <i>Hmga1</i> ^{fl/fl}	F	12.4	2225	131	Y	PDAC	Mostly necrotic
13	KPC/ <i>Hmga1</i> ^{fl/fl}	F	19.4	759	28.6	Y	PDAC	–
14	KPC/ <i>Hmga1</i> ^{fl/fl}	M	27.14	1840	74.8	Y	PDAC	Sarcomatoid carcinoma
1	KPC/ <i>Hmga1</i> ^{-/-}	M	22.1	211	9.7	N	No PDAC, focal ADM	Verrucous squamous proliferation in distal esophagus
2	KPC/ <i>Hmga1</i> ^{fl/fl}	F	31.9	1489	56.8	Y	PDAC	–
3	KPC/ <i>Hmga1</i> ^{fl/fl}	M	17.2	242	12.7	N	No tumor	Intestinal obstruction due to intestinal tumor; facial tumor present
4	KPC/ <i>Hmga1</i> ^{fl/fl}	M	22	606	22.8	Y	PDAC	–
5	KPC/ <i>Hmga1</i> ^{fl/fl}	M	22	779	29.3	Y	PDAC	–
6	KPC/ <i>Hmga1</i> ^{fl/fl}	F	16.14	3943	153.1	Y	Sarcomatoid carcinoma	Enlarged spleen, pancreatic tumors attached to abdominal wall; pancreatic tumor necrosis; enlarged thymus; growths throughout GI tract
7	KPC/ <i>Hmga1</i> ^{fl/fl}	M	17.4	185	8.9	NA	NA	–
8	KPC/ <i>Hmga1</i> ^{fl/fl}	M	36.7	1990	60.7	Y	PDAC	Hemorrhagic ascites

Panc, pancreas; PDAC, pancreatic ductal adenocarcinoma; ADM, acinar ductal metaplasia; LG, low-grade; PanIN, pancreatic intraepithelial neoplasia; F, female; M, male; NA, not applicable; N, no disease detected. ^AMouse died prior to necropsy.

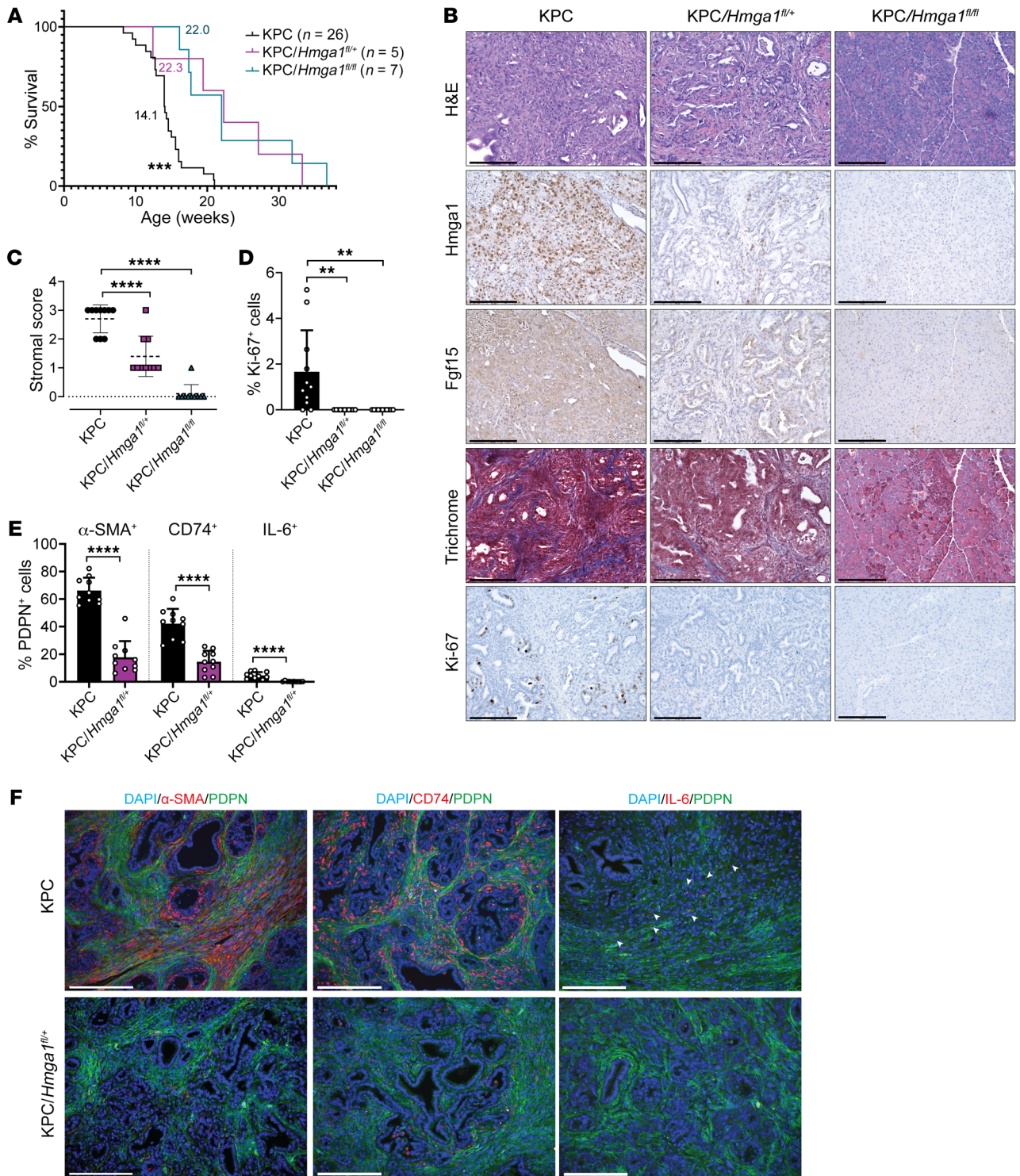


Figure 10. *Hmga1* haploinsufficiency within the pancreatic ductal epithelium is sufficient to mitigate tumorigenesis and fibrotic stroma formation in KPC mice. (A) Kaplan-Meier plot showing survival in KPC mice ($n = 26$, 11 males) compared to KPC with pancreatic ductal epithelial heterozygous *Hmga1* deficiency, KPC/*Hmga1*^{fl/+} ($n = 5$, 3 males), or KPC mice with pancreas-specific homozygous *Hmga1* deficiency KPC/*Hmga1*^{fl/fl} ($n = 7$, 5 males). Median survivals are indicated. (B) Representative images showing H&E (top row), HMGA1 (second row), FGF15 (third row), fibrosis (trichrome; fourth row), and Ki-67 (bottom row). Scale bars: 200 μm. (C) Comparison of stroma fibrosis scores in KPC models. (D) Comparison of Ki-67-positive cells in KPC models with or without pancreas-specific *Hmga1* deficiency. (E) CAF composition and (F) representative IF images in KPC models with or without pancreas-specific *Hmga1* deficiency. Total CAF number ascertained by costaining with DAPI and for PDPN; α-SMA, CD74, and IL-6 were used to identify percentages of total CAFs positive for each marker. In B–F, data were based on 5 fields at ×20 magnification of tumors from 2 mice/genotype, $n = 10$ per condition. Data presented as mean ± SD from independent mice. ** $P < 0.01$, *** $P < 0.001$, **** $P < 0.0001$ by log-rank (Mantel-Cox) test (A), 1-way ANOVA with Dunnett’s multiple-comparison test (C and D), or 2-tailed Student’s *t* test for α-SMA⁺ and CD74⁺ CAFs (data normally distributed) and Mann-Whitney test for IL-6⁺ CAFs (data not normally distributed) (E). Scale bars: 200 μm.

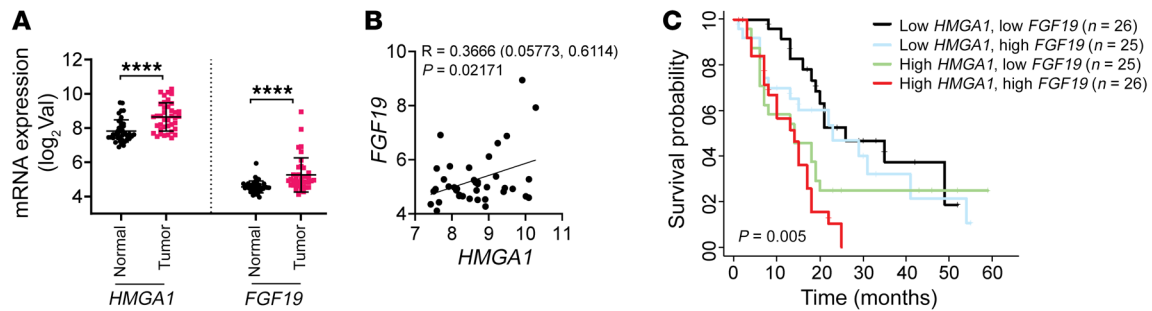


Figure 11. Overexpression of both *HMGA1* and *FGF19* in human PDAC defines a molecular subclass with extremely poor outcomes. (A) *HMGA1* and *FGF19* mRNA levels in paired nonmalignant tissue (labeled normal) and primary PDAC tumors (GSE15471); $n = 36$ for PDAC tumors and $n = 36$ for nonmalignant tissue. (B) *HMGA1* and *FGF19* expression is positively correlated in PDAC tumors (GSE15471; $n = 36$). (C) Kaplan-Meier plot showing poor overall survival of PDAC patients with both high *HMGA1* and *FGF19* expression (red, $n = 26$), high *HMGA1* and low *FGF19* expression (green, $n = 25$), low *HMGA1* and high *FGF19* expression (blue, $n = 25$), and low *HMGA1* and *FGF19* expression (black, $n = 26$) from GSE21501. Data presented as mean \pm SD. Significance was evaluated by 2-tailed Student's *t* test (A), Pearson's analysis (B), or log-rank (Mantel-Cox) test (C). **** $P < 0.0001$.

tially unique because it involves both tumor cell-intrinsic and microenvironmental interactions that collaborate during tumor progression. Intriguingly, we recently found that *HMGA1* causes bone marrow fibrosis during progression in mouse models of chronic myeloid malignancies (*JAK2^{V617F}* myeloproliferative neoplasms), suggesting that fibrosis mediated by *HMGA1* is relevant to diverse tumors (49). Importantly, *HMGA1* also regulates transcriptional networks involved in cell cycle progression (E2F targets, G₂/M checkpoint, mitotic spindle) in myeloid malignancies, although *FGF19* and bile acid metabolic genes are unique to PDAC cells. Surprisingly, silencing *FGF19* recapitulates most, but not all, phenotypes associated with *HMGA1* silencing, suggesting that it is an important transcriptional target, although other *HMGA1* transcriptional networks clearly contribute to PDAC carcinogenesis in our models.

Prior studies revealed mutations and epigenetic alterations that arise early in pancreatic carcinogenesis, although this has not impacted therapies (3). Less is known about later mechanisms driving progression. Clonal evolution studies suggest that PDACs evolve over many years, or even decades, which could foster clonal diversity and facilitate tumor progression (90). Another vexing characteristic of PDAC is the desmoplastic stroma composed of fibrotic scar tissue and CAFs, which also exhibit heterogeneity (9, 10). Although studies of CAF signaling and biophysical properties of stroma suggest that desmoplasia fuels tumor progression, the stroma restrains tumor growth in KPC models (7, 8). These studies, together with our results, suggest that the stroma has multiple functions, which may depend on tumor stage and properties of tumor cells, and stromal composition. The stroma could provide an initial barrier that is circumvented as tumor cells become more plastic (18). While we could not dissect the contribution of the stroma in isolation, our models suggest that *HMGA1* and *FGF19* collaborate to promote tumor progression and stroma formation. Because *HMGA1* proteins are detectable only in late-stage precursor lesions (pancreatic intraepithelial neoplasia [PanIN] 3) or invasive tumors, this mechanism may be relevant later in carcinogenesis when tumor cells invade and metastasize (38). Of note, we found lower frequencies of IL-6⁺ CAFs in KPC mice compared with other stud-

ies (19). Although the reason for this is unknown, inflammatory signals may vary in different mouse colonies from factors such as the microbiome. Despite these differences, however, tumors formed within a time frame similar to those of published studies with KPC mice. Together, our work reveals a therapeutic target relevant to a newly defined molecular subclass of human PDAC characterized by high expression of *HMGA1* and *FGF19*. Indeed, gene expression and survival data indicate that such tumors are among the most rapidly lethal PDACs.

FGF19 is a pleiotropic, hormone-like protein that regulates lipid, carbohydrate, and bile acid metabolism through the receptor *FGFR4* (72). Released from the ileum into enterohepatic circulation after exposure to bile salts in postprandial states, *FGF19* dampens further bile acid release (72). *FGF19* is also expressed in embryonic stem cells (91). In mice, *FGF15* is required for embryogenesis and liver regeneration (92), and *FGF15* induces hepatocellular carcinoma (HCC) when overexpressed in skeletal muscle, presumably through paracrine effects (71). *FGF19* is also overexpressed in human HCC harboring amplifications involving the *FGF19* locus (chromosome 11q13) (93), which led to the development of clinical inhibitors (64, 75–77). A recent study in HCC, however, showed only modest responses to an *FGFR4* inhibitor (75), although chemically induced HCC in mice with *Fgf15* deficiency show less fibrosis (74), suggesting that *FGF15* fosters fibrosis in HCC. *HMGA1* is also upregulated in human HCC (94, 95), and *FGF19* is overexpressed or amplified in other tumors with *HMGA1* overexpression (77). In a PDAC cell line, *GLI/ERK* signaling upregulates *FGF19* and xenograft tumorigenesis (96), and our GSEA analyses link *HMGA1* to *ERK* networks (Supplemental Table 1), consistent with *HMGA1* as a central hub through which multiple oncogenic pathways converge. In PDAC models, *FGF19* promotes tumor growth and stroma formation. Moreover, KPC mice with loss of a single *Hmga1* allele within pancreatic ductal epithelium exhibit increased tumor latency, less fibrosis, and decreased *FGF15* immunoreactivity, further supporting a collaborative role for *HMGA1* and *FGF15* in tumorigenesis and fibrotic desmoplasia (Figure 10, B and C).

In human PDAC, *FGF19* expression is more variable than *HMGA1*, the latter of which is upregulated in most tumors (36,

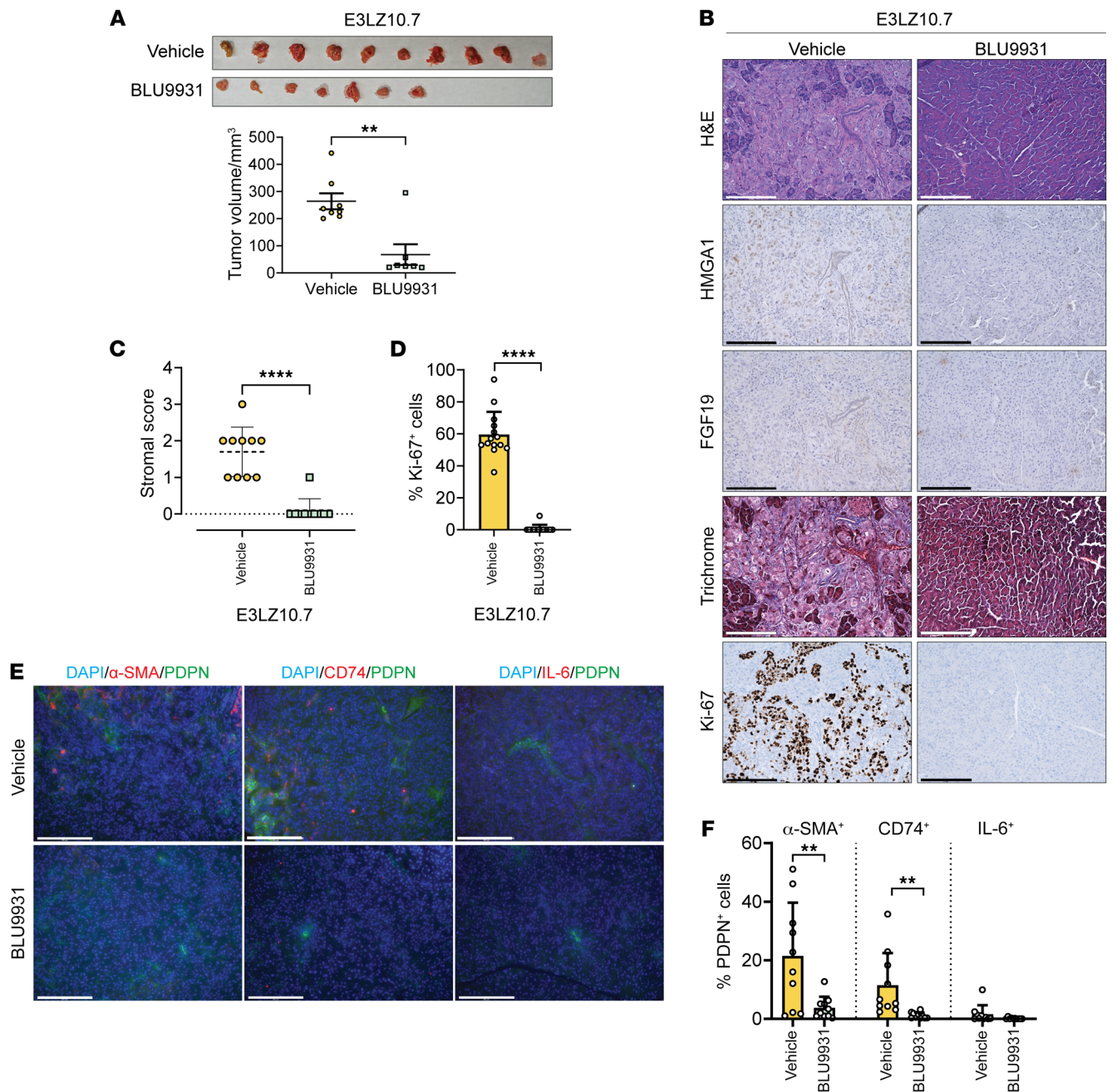


Figure 12. FGFR4 inhibition with BLU9931 decreases tumorigenesis and stroma formation in human PDAC orthotopic implants. (A) Tumors (top) and volume comparisons (bottom) from orthotopic implantation of E3LZ10.7 cells in mice treated with BLU9931 or vehicle control. Data presented as mean \pm SEM. (B) Representative images ($n = 10$ per condition) of tumors stained with H&E (top row) and for HMGA1 (second row), FGF19 (third row), fibrosis (trichrome; fourth row), and Ki-67 (bottom row) in E3LZ10.7 orthotopic implants of mice treated with BLU9931 or vehicle. (C) Comparison of stromal fibrosis scores in E3LZ10.7 orthotopic implants based on a 3-point system. (D) Comparison of Ki-67⁺ cells in E3LZ10.7 orthotopic implants of mice treated with BLU9931 or with vehicle control. (E) Representative IF images of CAFs in E3LZ10.7 orthotopic implants of mice treated with BLU9931 or with vehicle. (F) Comparison of CAFs in E3LZ10.7 orthotopic implants of mice treated with BLU9931 or vehicle. Total CAF number ascertained by costaining with DAPI and for PDPN; α -SMA, CD74, and IL-6 were used to identify percentage of total CAFs positive for each marker. Data in C–D were based on 10 fields from 3 different mice/group at $\times 20$ magnification ($n = 10$ /condition); data in E were based on 10 fields from 1 mouse/group at $\times 20$ magnification ($n = 10$ /condition). Data presented as mean \pm SD (C, D, and F). Significance was evaluated by Mann-Whitney test (A, C, and D) or 2-tailed Student's *t* test for α -SMA⁺ and CD74⁺ CAFs (data normally distributed) and Mann-Whitney for IL-6⁺ CAFs (data not normally distributed) (F). ***P* < 0.01, *****P* < 0.0001. Scale bars: 200 μ m.

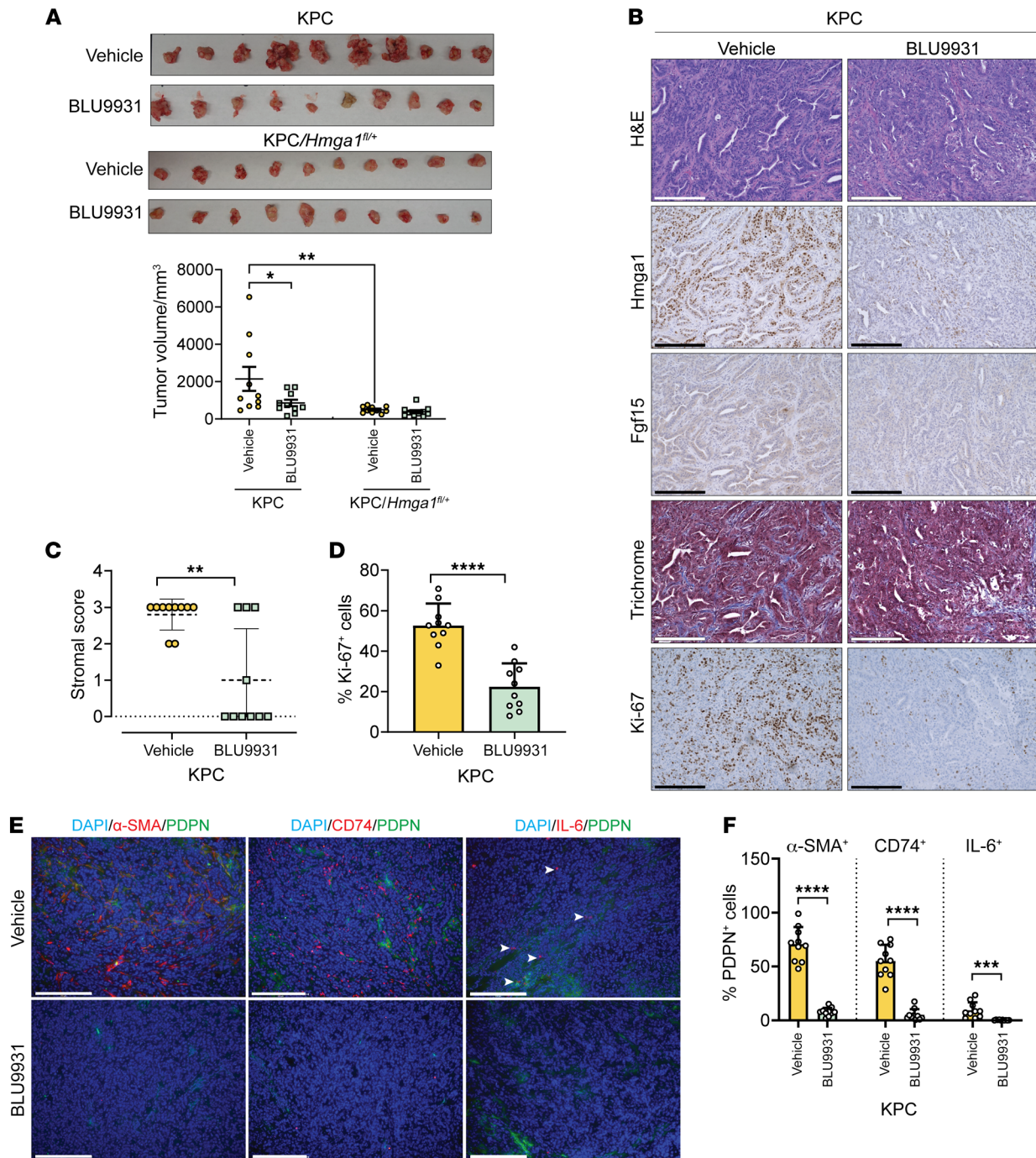


Figure 13. BLU9931 mitigates tumorigenesis and stroma formation in orthotopic implants from KPC PDAC cells. (A) Tumors (top) and volume comparisons (bottom) from orthotopic implantation of KPC xenografts mice treated with BLU9931 or vehicle control. Data presented as mean \pm SEM. (B) Representative images ($n = 10$ per condition) of tumors stained with H&E (top row) and for HMGA1 (second row), FGF15 (third row), fibrosis (trichrome, fourth row), and Ki-67 (fifth row) in KPC orthotopic implants of mice treated with BLU9931 or vehicle control. (C) Stromal fibrosis scores shown as violin plots in KPC orthotopic implants based on a 3-point system. (D) Comparison of Ki-67⁺ cells in KPC orthotopic implants of mice treated with BLU9931 or vehicle control. (E) Representative IF images of CAFs. (F) Comparison of CAFs in KPC orthotopic implants of mice treated with BLU9931 or vehicle control. Total CAF number ascertained by costaining with DAPI and for PDPN; α -SMA, CD74, and IL-6 were used to identify different subtypes of CAFs positive for each marker. Data in C–D were based on 10 fields from 3 different mice/group at x20 magnification ($n = 10$ /condition); data in E were based on 10 fields from 1 mouse/group at x20 magnification ($n = 10$ /condition). Data presented as mean \pm SD (C, D, and F). Significance was evaluated by Significance was evaluated by 1-way ANOVA with Tukey’s multiple-comparison test (A), Mann-Whitney test (C), 2-tailed Student’s *t* test (D), or 2-tailed Student’s *t* test for α -SMA⁺ and CD74⁺ CAFs (data normally distributed) and Mann-Whitney test for IL-6⁺ CAFs (data not normally distributed) (F). * $P < 0.05$, ** $P < 0.01$, *** $P < 0.001$, **** $P < 0.0001$.

38). Why *FGF19* is induced in only a fraction of tumors remains unclear. Pancreatic carcinogenesis may proceed through step-wise accumulation of mutations, or chromothripsis, whereby thousands of clustered chromosomal rearrangements occur simultaneously (3, 97). The complex genome likely contributes to PDAC heterogeneity, and some genetic alterations may affect *FGF19* expression. Notably, *FGF19* only partially restores proliferation in cells with *HMGA1* silencing, indicating that other *HMGA1* pathways foster tumorigenesis. Our transcriptomes reveal multiple *HMGA1* pathways and further investigation could reveal other actionable mechanisms. However, *FGF19* deficiency recapitulates most effects of *HMGA1* silencing and our KPC studies are consistent with *FGF15* as a downstream *HMGA1* effector. Despite the circumscribed population of human tumors with both *HMGA1* and *FGF19* overexpression, these data delineate a molecular subclass with worse outcomes that could be targeted in therapy (98).

KRAS-driven tumors, and PDAC in particular, have proven formidable therapeutic challenges. Therapies that target KRAS are emerging, although their efficacy in PDAC is unknown (99, 100). While inhibitors of chromatin regulators, such as bromodomain proteins, show efficacy, successes in PDAC are lacking (101). Growth factors provide attractive targets because they can be neutralized by antibodies or receptor blockade. Our work illuminates *HMGA1* and *FGF19* as key players in PDAC tumorigenesis and stroma formation. Most importantly, this pathway is conserved in a subset of human tumors with exceptionally poor outcomes. Together, we discovered what we believe is a previously undescribed paradigm whereby tumor cells collaborate via *HMGA1* and *FGF19* to drive progression, thus illuminating *FGF19* as a rational therapeutic target for a molecular subclass composed of the most aggressive human PDACs.

Methods

Detailed methods, statistical analyses, and reagents are provided in the supplemental material, including culture medium, primers, and antibodies (Supplemental Tables 2–4). RNA sequencing data were deposited into the NCI Gene Expression Omnibus (GEO GSE222890). See complete unedited blots in the supplemental material.

Author contributions

LR conceptualized the project. LC and BW drafted parts of the manuscript, and LR wrote the final draft, which was reviewed by all authors prior to submission. LC, BW, JHK, LZL, SS, IH, SYC, LL, LX, TH, MH, WJS, SI, GG, LMC, KG, LW, and LR performed experiments and analyzed data. EJ, LZ, KR, KG, and LMC provided reagents and guidance with experiments. LW, BW, LC, LZL, and WJS interpreted histology.

Acknowledgments

This research was supported by the NIH (R01 CA232741, R01 HL145780, R01 DK102943, R01 HL143818, R03 CA182679, R03 CA191621), Allegheny-Health Network, Maryland Stem Cell Research Fund, and the Sol Goldman Pancreatic Cancer Research Center. This work is dedicated to the memory of LR's father, Larry C. Smith, and all patients with pancreatic cancer in need of better therapies.

Address correspondence to: Linda Resar, Johns Hopkins University SOM, 720 Rutland Avenue, Ross Research Building, Room 1025, Baltimore, Maryland, 21205, USA. Phone: 410.614.0712; Email: lresar@jhmi.edu.

WJS's present address is: Department of Pathology, Catholic University of Daegu, Daegu, South Korea.

- Kleeff J, et al. Pancreatic cancer. *Nat Rev Dis Primers*. 2016;2:16022.
- Siegel RL, et al. Cancer statistics, 2020. *CA Cancer J Clin*. 2020;70(1):7–30.
- Wood LD, et al. Genetics of familial and sporadic pancreatic cancer. *Gastroenterology*. 2019;156(7):2041–2055.
- Collisson EA, et al. Molecular subtypes of pancreatic cancer. *Nat Rev Gastroenterol Hepatol*. 2019;16(4):207–220.
- Waddell N, et al. Whole genomes redefine the mutational landscape of pancreatic cancer. *Nature*. 2015;518(7540):495–501.
- Whatcott CJ, et al. Desmoplasia in primary tumors and metastatic lesions of pancreatic cancer. *Clin Cancer Res*. 2015;21(15):3561–3568.
- Özdemir BC, et al. Depletion of carcinoma-associated fibroblasts and fibrosis induces immunosuppression and accelerates pancreatic cancer with reduced survival. *Cancer Cell*. 2014;25(6):719–734.
- Rhim AD, et al. Stromal elements act to restrain, rather than support, pancreatic ductal adenocarcinoma. *Cancer Cell*. 2014;25(6):735–747.
- Ligorio M, et al. Stromal microenvironment shapes the intratumoral architecture of pancreatic cancer. *Cell*. 2019;178(1):160–175.e27.
- Ho WJ, et al. The tumour microenvironment in pancreatic cancer - clinical challenges and opportunities. *Nat Rev Clin Oncol*. 2020;17(9):527–540.
- Gieniec KA, et al. Cancer-associated fibroblasts-heroes or villains? *Br J Cancer*. 2019;121(4):293–302.
- Ho WJ, Jaffee EM. Disrupting a converging metabolic target turns up the immunologic-heat in pancreatic tumors. *J Clin Invest*. 2020;130(1):200–273.
- Joyce JA, Fearon DT. T cell exclusion, immune privilege, and the tumor microenvironment. *Science*. 2015;348(6230):74–80.
- Su S, et al. CD10⁺GPR77⁺ cancer-associated fibroblasts promote cancer formation and chemoresistance by sustaining cancer stemness. *Cell*. 2018;172(4):841–856.
- Gilkes DM, et al. Hypoxia and the extracellular matrix: drivers of tumour metastasis. *Nat Rev Cancer*. 2014;14(6):430–439.
- Xiao Q, et al. Cancer-associated fibroblasts in pancreatic cancer are reprogrammed by tumor-induced alterations in genomic DNA methylation. *Cancer Res*. 2016;76(18):5395–5404.
- Provenzano PP, et al. Enzymatic targeting of the stroma ablates physical barriers to treatment of pancreatic ductal adenocarcinoma. *Cancer Cell*. 2012;21(3):418–429.
- Bulle A, Lim KH. Beyond just a tight fortress: contribution of stroma to epithelial-mesenchymal transition in pancreatic cancer. *Signal Transduct Target Ther*. 2020;5(1):249.
- Elyada E, et al. Cross-species single-cell analysis of pancreatic ductal adenocarcinoma reveals antigen-presenting cancer-associated fibroblasts. *Cancer Discov*. 2019;9(8):1102–1123.
- Öhlund D, et al. Distinct populations of inflammatory fibroblasts and myofibroblasts in pancreatic cancer. *J Exp Med*. 2017;214(3):579–596.
- Feig C, et al. Targeting CXCL12 from FAP-expressing carcinoma-associated fibroblasts synergizes with anti-PD-L1 immunotherapy in pancreatic cancer. *Proc Natl Acad Sci U S A*. 2013;110(50):20212–20217.
- Neuzillet C, et al. Inter- and intra-tumoural heterogeneity in cancer-associated fibroblasts of human pancreatic ductal adenocarcinoma. *J Pathol*. 2019;248(1):51–65.
- Helms EJ, et al. Mesenchymal lineage heterogeneity underlies nonredundant functions of pancreatic cancer-associated fibroblasts. *Cancer Discov*. 2022;12(2):484–501.
- Reddy KL, Feinberg AP. Higher order chromatin organization in cancer. *Semin Cancer Biol*. 2013;23(2):109–115.
- Ryan DP, et al. Pancreatic adenocarcinoma. *N Engl J Med*. 2014;371(11):1039–1049.

26. Ueki T, et al. Hypermethylation of multiple genes in pancreatic adenocarcinoma. *Cancer Res.* 2000;60(7):1835-1839.
27. Sato N, et al. Frequent hypomethylation of multiple genes overexpressed in pancreatic ductal adenocarcinoma. *Cancer Res.* 2003;63(14):4158-4166.
28. Omura N, et al. Genome-wide profiling of methylated promoters in pancreatic adenocarcinoma. *Cancer Biol Ther.* 2008;7(7):1146-1156.
29. Kugel S, et al. SIRT6 suppresses pancreatic cancer through control of Lin28b. *Cell.* 2016;165(6):1401-1415.
30. Ben-Porath I, et al. An embryonic stem cell-like gene expression signature in poorly differentiated aggressive human tumors. *Nat Genet.* 2008;40(5):499-507.
31. Reeves R, Beckerbauer L. HMG1/Y proteins: flexible regulators of transcription and chromatin structure. *Biochim Biophys Acta.* 2001;1519(1-2):13-29.
32. Xu Y, et al. The HMG-I oncogene causes highly penetrant, aggressive lymphoid malignancy in transgenic mice and is overexpressed in human leukemia. *Cancer Res.* 2004;64(10):3371-3375.
33. Tesfaye A, et al. The high-mobility group A1 gene up-regulates cyclooxygenase 2 expression in uterine tumorigenesis. *Cancer Res.* 2007;67(9):3998-4004.
34. Hock R, et al. HMG chromosomal proteins in development and disease. *Trends Cell Biol.* 2007;17(2):72-79.
35. Hillion J, et al. The high-mobility group A1a/signal transducer and activator of transcription-3 axis: an Achilles heel for hematopoietic malignancies? *Cancer Res.* 2008;68(24):10121-10127.
36. Liao S-S, et al. High mobility group AT-hook 1 (HMGA1) is an independent prognostic factor and novel therapeutic target in pancreatic adenocarcinoma. *Cancer.* 2008;113(2):302-314.
37. Hillion J, et al. Upregulation of MMP-2 by HMGA1 promotes transformation in undifferentiated, large-cell lung cancer. *Mol Cancer Res.* 2009;7(11):1803-1812.
38. Hristov AC, et al. HMGA1 correlates with advanced tumor grade and decreased survival in pancreatic ductal adenocarcinoma. *Mod Pathol.* 2010;23(1):98-104.
39. Resar LMS. The high mobility group A1 gene: transforming inflammatory signals into cancer? *Cancer Res.* 2010;70(2):436-439.
40. Nelson DM, et al. Flavopiridol induces BCL-2 expression and represses oncogenic transcription factors in leukemic blasts from adults with refractory acute myeloid leukemia. *Leuk Lymphoma.* 2011;52(10):1999-2006.
41. Karp JE, et al. Phase I and pharmacologic trial of cytosine arabinoside with the selective checkpoint 1 inhibitor Sch 900776 in refractory acute leukemias. *Clin Cancer Res.* 2012;18(24):6723-6731.
42. Belton A, et al. HMGA1 induces intestinal polyposis in transgenic mice and drives tumor progression and stem cell properties in colon cancer cells. *PLoS One.* 2012;7(1):e30034.
43. Di Cello F, et al. Inactivation of the Cdkn2a locus cooperates with HMGA1 to drive T-cell leukemogenesis. *Leuk Lymphoma.* 2013;54(8):1762-1768.
44. Roy S, et al. HMGA1 overexpression correlates with relapse in childhood B-lineage acute lymphoblastic leukemia. *Leuk Lymphoma.* 2013;54(11):2565-2567.
45. Hillion J, et al. The high mobility group A1 (HMGA1) gene is highly overexpressed in human uterine serous carcinomas and carcinosarcomas and drives matrix metalloproteinase-2 (MMP-2) in a subset of tumors. *Gynecol Oncol.* 2016;141(3):580-587.
46. Xian L, et al. HMGA1 amplifies Wnt signalling and expands the intestinal stem cell compartment and Paneth cell niche. *Nat Commun.* 2017;8:15008.
47. Resar L, et al. Lessons from the crypt: HMGA1-amping up Wnt for stem cells and tumor progression. *Cancer Res.* 2018;78(8):1890-1897.
48. Gorbounov M, et al. High mobility group A1 (HMGA1) protein and gene expression correlate with ER-negativity and poor outcomes in breast cancer. *Breast Cancer Res Treat.* 2020;179(1):25-35.
49. Li L, et al. HMGA1 chromatin regulators induce transcriptional networks involved in GATA2 and proliferation during MPN progression. *Blood.* 2022;139(18):2797-2815.
50. Liao SS, Whang E. High mobility group A: a novel biomarker and therapeutic target in pancreatic adenocarcinoma. *Surgeon.* 2009;7(5):297-306.
51. Shah SN, et al. HMGA1 reprograms somatic cells into pluripotent stem cells by inducing stem cell transcriptional networks. *PLoS One.* 2012;7(11):e48533.
52. Chou BK, et al. Efficient human iPS cell derivation by a non-integrating plasmid from blood cells with unique epigenetic and gene expression signatures. *Cell Res.* 2011;21(3):518-529.
53. Schuldenfrei A, et al. HMGA1 drives stem cell, inflammatory pathway, and cell cycle progression genes during lymphoid tumorigenesis. *BMC Genomics.* 2011;12:549.
54. Lanahan A, et al. Growth factor-induced delayed early response genes. *Mol Cell Biol.* 1992;12(9):3919-3929.
55. Holth LT, et al. Effects of epidermal growth factor and estrogen on the regulation of the HMG-I/Y gene in human mammary epithelial cell lines. *DNA Cell Biol.* 1997;16(11):1299-1309.
56. Veite-Schmahl MJ, et al. HMGA1 expression levels are elevated in pancreatic intraepithelial neoplasia cells in the Ptf1a-Cre; LSL-KrasG12D transgenic mouse model of pancreatic cancer. *Br J Cancer.* 2017;117(5):639-647.
57. Zeitels LR, et al. Tumor suppression by miR-26 overrides potential oncogenic activity in intestinal tumorigenesis. *Genes Dev.* 2014;28(23):2585-2590.
58. Wood LJ, et al. HMG-I/Y, a new c-Myc target gene and potential oncogene. *Mol Cell Biol.* 2000;20(15):5490-5502.
59. Dhar A, et al. Dominant-negative c-Jun (TAM67) target genes: HMGA1 is required for tumor promoter-induced transformation. *Oncogene.* 2004;23(25):4466-4476.
60. Hommura F, et al. HMG-I/Y is a c-Jun/activator protein-1 target gene and is necessary for c-Jun-induced anchorage-independent growth in Rat1a cells. *Mol Cancer Res.* 2004;2(5):305-314.
61. Hillion J, et al. The HMGA1-COX-2 axis: a key molecular pathway and potential target in pancreatic adenocarcinoma. *Pancreatol.* 2012;12(4):372-379.
62. Liao S-S, et al. HMGA1 is a determinant of cellular invasiveness and in vivo metastatic potential in pancreatic adenocarcinoma. *Cancer Res.* 2006;66(24):11613-11622.
63. Hingorani SR, et al. Trp53R172H and KrasG12D cooperate to promote chromosomal instability and widely metastatic pancreatic ductal adenocarcinoma in mice. *Cancer Cell.* 2005;7(5):469-483.
64. Hagel M, et al. First selective small molecule inhibitor of FGFR4 for the treatment of hepatocellular carcinomas with an activated FGFR4 signaling pathway. *Cancer Discov.* 2015;5(4):424-437.
65. Lee KM, et al. Immortalization with telomerase of the Nestin-positive cells of the human pancreas. *Biochem Biophys Res Commun.* 2003;301(4):1038-1044.
66. Embuscado EE, et al. Immortalizing the complexity of cancer metastasis: genetic features of lethal metastatic pancreatic cancer obtained from rapid autopsy. *Cancer Biol Ther.* 2005;4(5):548-554.
67. Moore PS, et al. Genetic profile of 22 pancreatic carcinoma cell lines. Analysis of K-ras, p53, p16 and DPC4/Smad4. *Virchows Arch.* 2001;439(6):798-802.
68. Love MI, et al. Moderated estimation of fold change and dispersion for RNA-seq data with DESeq2. *Genome Biol.* 2014;15(12):550.
69. Subramanian A, et al. Gene set enrichment analysis: a knowledge-based approach for interpreting genome-wide expression profiles. *Proc Natl Acad Sci U S A.* 2005;102(43):15545-15550.
70. Mootha VK, et al. PGC-1alpha-responsive genes involved in oxidative phosphorylation are coordinately downregulated in human diabetes. *Nat Genet.* 2003;34(3):267-273.
71. Nicholes K, et al. A mouse model of hepatocellular carcinoma: ectopic expression of fibroblast growth factor 19 in skeletal muscle of transgenic mice. *Am J Pathol.* 2002;160(6):2295-2307.
72. Wu A-L, et al. FGF19 regulates cell proliferation, glucose and bile acid metabolism via FGFR4-dependent and independent pathways. *PLoS One.* 2011;6(3):e17868.
73. Miura S, et al. Fibroblast growth factor 19 expression correlates with tumor progression and poorer prognosis of hepatocellular carcinoma. *BMC Cancer.* 2012;12:56.
74. Uriarte I, et al. Ileal FGF15 contributes to fibrosis-associated hepatocellular carcinoma development. *Int J Cancer.* 2015;136(10):2469-2475.
75. Kim RD, et al. First-in-human phase I study of fisolatinib (BLU-554) validates aberrant FGF19 signaling as a driver event in hepatocellular carcinoma. *Cancer Discov.* 2019;9(12):1696-1707.
76. Lang L, Teng Y. Fibroblast growth factor receptor 4 targeting in cancer: new insights into mechanisms and therapeutic strategies. *Cells.* 2019;8(1):31.
77. Levine KM, et al. FGFR4: A promising therapeutic target for breast cancer and other solid tumors. *Pharmacol Ther.* 2020;214:107590.
78. Cartharius K, et al. MatInspector and beyond: promoter analysis based on transcription factor binding sites. *Bioinformatics.* 2005;21(13):2933-2942.
79. Creighton MP, et al. Histone H3K27ac separates active from poised enhancers and predicts developmental state. *Proc Natl Acad Sci U S A.*

- 2010;107(50):21931-21936.
80. Wainwright EN, Scaffidi P. Epigenetics and cancer stem cells: unleashing, hijacking, and restricting cellular plasticity. *Trends Cancer*. 2017;3(5):372-386.
81. Himes SR, et al. The role of high-mobility group I(Y) proteins in expression of IL-2 and T cell proliferation. *J Immunol*. 2000;164(6):3157-3168.
82. Badea L, et al. Combined gene expression analysis of whole-tissue and microdissected pancreatic ductal adenocarcinoma identifies genes specifically overexpressed in tumor epithelia. *Hepatogastroenterology*. 2008;55(88):2016-2027.
83. Pei H, et al. FKBP51 affects cancer cell response to chemotherapy by negatively regulating Akt. *Cancer Cell*. 2009;16(3):259-266.
84. Stratford JK, et al. A six-gene signature predicts survival of patients with localized pancreatic ductal adenocarcinoma. *PLoS Med*. 2010;7(7):e1000307.
85. Flavahan WA, et al. Epigenetic plasticity and the hallmarks of cancer. *Science*. 2017;357(6348):eaal2380.
86. Morgan MA, Shilatifard A. Chromatin signatures of cancer. *Genes Dev*. 2015;29(3):238-249.
87. Feinberg AP, et al. Epigenetic modulators, modifiers and mediators in cancer aetiology and progression. *Nat Rev Genet*. 2016;17(5):284-299.
88. Shah SN, et al. HMGA1: a master regulator of tumor progression in triple-negative breast cancer cells. *PLoS One*. 2013;8(5):e63419.
89. Sumter TF, et al. The high mobility group A1 (HMGA1) transcriptome in cancer and development. *Curr Mol Med*. 2016;16(4):353-393.
90. Peng J, et al. Single-cell RNA-seq highlights intra-tumoral heterogeneity and malignant progression in pancreatic ductal adenocarcinoma. *Cell Res*. 2019;29(9):725-738.
91. Krejci P, et al. Expression of FGF19 in human embryonic stem cells. *Stem Cells*. 2013;31(11):2582-2584.
92. Kong B, et al. Fibroblast growth factor 15 deficiency impairs liver regeneration in mice. *Am J Physiol Gastrointest Liver Physiol*. 2014;306(10):G893-G902.
93. Sawey ET, et al. Identification of a therapeutic strategy targeting amplified FGF19 in liver cancer by oncogenomic screening. *Cancer Cell*. 2011;19(3):347-358.
94. Chuma M, et al. Expression profiling in hepatocellular carcinoma with intrahepatic metastasis: identification of high-mobility group I(Y) protein as a molecular marker of hepatocellular carcinoma metastasis. *Keio J Med*. 2004;53(2):90-97.
95. Andreozzi M, et al. HMGA1 expression in human hepatocellular carcinoma correlates with poor prognosis and promotes tumor growth and migration in in vitro models. *Neoplasia*. 2016;18(12):724-731.
96. Eberl M, et al. Hedgehog-EGFR cooperation response genes determine the oncogenic phenotype of basal cell carcinoma and tumour-initiating pancreatic cancer cells. *EMBO Mol Med*. 2012;4(3):218-233.
97. Stephens PJ, et al. Massive genomic rearrangement acquired in a single catastrophic event during cancer development. *Cell*. 2011;144(1):27-40.
98. Degirolamo C, et al. Therapeutic potential of the endocrine fibroblast growth factors FGF19, FGF21 and FGF23. *Nat Rev Drug Discov*. 2016;15(1):51-69.
99. McCormick F. KRAS as a therapeutic target. *Clin Cancer Res*. 2015;21(8):1797-1801.
100. Salgia R, et al. The improbable targeted therapy: KRAS as an emerging target in non-small cell lung cancer (NSCLC). *Cell Rep Med*. 2021;2(1):100186.
101. Stathis A, Bertoni F. BET proteins as targets for anticancer treatment. *Cancer Discov*. 2018;8(1):24-36.
102. Hu Y, Smyth GK. ELDA: extreme limiting dilution analysis for comparing depleted and enriched populations in stem cell and other assays. *J Immunol Methods*. 2009;347(1-2):70-78.